MUSCLE SYNERGIES: EXTRACTION AND IMPLEMENTATION IN UPPER LIMB MOVEMENT CONTROL

PHAM THI THU HANG

MARCH 2013

MUSCLE SYNERGIES: EXTRACTION AND IMPLEMENTATION IN UPPER LIMB MOVEMENT CONTROL

A dissertation submitted to

THE GRADUATE SCHOOL OF ENGINEERING SCIENCE

OSAKA UNIVERSITY

in partial fulfillment of the requirements for the degree of

DOCTOR OF PHILOSOPHY IN ENGINEERING

BY

PHAM THI THU HANG

MARCH 2013

ABSTRACT

Robots, especially human-like robots, become more popular these days. They involve in many fields of human life, such as in manufacturing and in rehabilitations. Solving the redundancy problem is a key issue to improve the dexterity and stability of robots' performance so that they can work compliantly and safely with humans. This requires an understanding of the neuro-mechanical control of limb movements, which is necessary to integrate biological information with the mechanical system into a single architecture that is more flexible and more adaptive to a variety of environments. This understanding is also needed for the effective design of interfaces to transfer the skillful movements of humans to robots.

The synergy hypothesis suggests muscle synergies as a solution to the redundancy problem. On the other hand, the equilibrium point hypothesis is a promising hypothesis in motor control to interpret the physiology of movements. Inspired by the synergy hypothesis and the equilibrium-point hypothesis, we proposed two concepts, the agonist-antagonist (A-A) ratio and A-A activity, as variables to investigate muscle synergies. The derivation of the A-A ratio and A-A activity concepts was based on the analogy between the biological system and a robot system with antagonistic artificial muscles. The A-A ratio is directly and linearly related to the equilibrium joint angle for a desired motion. The A-A activity is directly and linearly associated with the joint stiffness at any equilibrium joint angle. We expected that these concepts would be applicable to the biological system, providing variables to extract muscle synergies from muscle activities.

We then provided a method to extract and implement muscle synergies from the human electromyography (EMG) for human upper limb movements. We conducted a hand-force

production task to investigate the mechanisms of the human's skillful hand-movement at producing force while manipulating objects. Using principle component analysis (PCA) algorithm, we reduced the dimension of the EMG dataset. Furthermore, using a linear regression analysis, we estimated the hand-force deviation in response to the reduced data of the measured EMGs with the constraint that all muscle contractions were isometric. A high correlation between the EMGs and the hand-forces was observed. From the regression model, muscle synergies can be extracted. While other methods cannot clarify the mechanisms of how the synergies generate forces, we can explain physical meanings of the extracted muscle synergies. Considering a polar coordinate frame centered on the shoulder joint, one synergy seemed to generate hand-forces in the angular direction, while the other synergy seemed to create hand-forces in the radial direction. This interpretation suggests a simple method to generate desired movements through two synergies resulted from a unique combination of multiple muscles.

Based on the human analysis results of the hand-force production task, we hypothesized a framework for motor control of the human upper limb. The framework suggests a simple and unique solution to generate upper limb movements. To implement the framework to musculoskeletal robot control, we proposed a synergy-based control method using two synergies as manipulated variables. This synergy control method is simple and flexible to be applicable to more complicated musculoskeletal robotic systems and for a wide range of tasks.

Last but not least, we conducted experiments to observe the performance of two human subjects in a coordinated task. The observed role sharing would be helpful to improve the performance of musculoskeletal robots that involve in interaction tasks with human.

ACKNOWLEDGEMENTS

First and foremost, I would like to express my sincere gratitude to my supervisor Prof. Fumio Miyazaki for his instructions, ideas, and wise advices to complete this thesis. He was always patient and very warm to me. He gave me lots of encouragements and helped me with all of his ability. He gave me many opportunities to learn, to experience, and to play as well. With his great help and orientation, I have gained much knowledge about the interesting bio-inspired robots. I feel lucky to be a student in his lab.

I would strongly like to thank Prof. Masao Tanaka and Prof. Tatsuo Arai for their critical reviewing of this thesis as well as their valuable suggestions.

I am very grateful to the support of Assoc. Prof. Hiroaki Hirai and Assis. Prof. Mistunori Uemura. They gave me many technical assistances and useful advices. I would also gratefully like to thank Prof. Atsushi Nishikawa for his understanding and support. I would like to thank Ms. Noriko Deguchi and other staffs for their understanding and flexible support during my course.

I would like to thank the lab-mates: Youhei Ariga, Takashi Kawai, Takanori Oku, Daisuke Maeda, Naoto Hasegawa, Keita Sasaki, and Taishi Fukushima. Ariga gave me great helps for programming and many other assistances. His master thesis was a big help for completing this work. Fukushima gave me many helps in understanding information in Japanese. The others spent a lot of time to carry out the experiments for this thesis. I would also like to thank other lab-mates, especially the two sweet girls Yuki Horise and Kanna Nakayama, for a friendly environment in the laboratory that made the research life less tough.

I would sincerely like to thank the Ministry of Education, Culture, Sport, Science and Technology of Japan (MEXT) for giving me the opportunity to study in Osaka University.

I would also deeply like to thank the Japan Society for the Promotion of Science for Young Scientists (JSPS) for giving me the chance to study abroad in the U.S., from which I gained lots of interesting experiences.

Finally, I would like to give my love to my family, who is always behind me and loves me tenderly. The utmost encouragement of the family gave me strength to face difficult times.

TABLE OF CONTENTS

LIST OF TABLES

LIST OF FIGURES

LIST OF ABBREVIATIONS

A-A activity	muscle activity of agonist-antagonist muscles pair.
A-A ratio	muscle ratio of agonist-antagonist muscles pair.
aPC1	the first principal component of A-A activity.
aPC2	the second principal component of A-A activity.
CNS	Central Nervous System.
EMG	Electromyography.
EP	equilibrium point.
PAM	pneumatic artificial muscle.
PC	principle component.
PCA	Principle Component Analysis.
rPC1	the first principal component of A-A ratio.
rPC2	the second principal component of A-A ratio.

CHAPTER I

INTRODUCTION

1.1 Introduction

Robotics plays an important role in many areas of human life. One of its important applications is in rehabilitation. Robots are expected to contribute to motor training in neurologically impaired patients by repeatedly guiding correct behavioral movements, to support elderly and disabled people by amplifying muscle forces, and to provide other services to assist in rehabilitation, such as haptic devices. There is a need to improve the dexterity and stability of robots so that they can work compliantly and safely with humans. This requires an understanding of the neuro-mechanical control of limb movements, which is necessary to integrate biological information with the mechanical system into a single architecture that is more flexible and more adaptive to a variety of environments. This understanding is also needed for the effective design of interfaces to transfer the skillful movements of humans to robots.

The flexibility of human movement is governed by the redundant degrees-of-freedom problem posed by Bernstein [32]. The movements we make, even the simplest ones, are the result of the coordinated actions of multiple muscles and joints across the limbs and trunk. The redundancy of degrees of freedom caused by multiple muscles and joints produces numerous possible solutions to a given task. Moreover, similar joint trajectories can be created by different muscle activation patterns [14]. This biomechanical redundancy requires the central nervous system (CNS) to solve the problem of choosing a unique solution to control the task-variables. In addition, the physiological mechanism of how the brain controls muscles still remains unknown. There are several hypotheses to explain how the CNS uniquely specifies control commands to each muscle and joint and how to interpret

the nature of the physiological control of the muscles by the brain.

The synergy hypothesis suggests muscle synergies as a solution to the redundancy problem [3, 11]. Bernstein first suggested that the CNS might simplify the control of movement by coupling small groups of muscles into more global units, thus reducing the number of controlled variables [32]. Many researchers have experimentally supported the idea that the CNS can generate a wide range of behavioral movements by combining groups of muscles, or muscle synergies [2, 12, 19, 25, 41, 46]. In addition, Ting [26] used muscle synergies to explain the mechanism of the transformation of neural commands into specific muscle activation patterns related to task-level variables. Muscle synergies transform the desired control of task variables into high-dimensional muscle activations to produce biomechanical outputs that generate sensory signals mapping onto task-variables. This framework presented the hierarchal control that the CNS uses to regulate muscle synergies, which reflect task-variable information.

A promising hypothesis in motor control to interpret the physiology of movements is the equilibrium-point (EP) hypothesis (λ model) proposed by Feldman [4]. According to this hypothesis, the CNS sends motor commands, each consisting of a reciprocal command and a co-activation command, to peripheral muscles to select a desired equilibrium position and its apparent stiffness. The reciprocal command is associated with the change in the equilibrium position. The co-activation command is related to the change in the stiffness. In order to produce behavior, the CNS has to translate task-level goals (the input) into these motor commands (the output). Because the input is generally low-dimensional compared to the output, an apparent problem of redundancy exists in this translation that may be involved in creating muscle synergies. Unfortunately, analysis of the translation between task-level goals and motor commands has been difficult due to the fact that the observed variables, such as forces and displacements, are indirect reflections of equilibrium trajectories [30]. The ambiguous relationship between the EP hypothesis and the notion of synergies is another problem at the moment.

1.2 Background and scope of the dissertation

There has been a large amount of research examining motor synergies using statistical analyses of electromyography (EMG) during behavior, without considering the EP hypothesis. These conventional experiments commonly tried to measure EMGs, to analyze EMGs using statistical methods, to evaluate the combination of extracted synergies, and to link the identified synergies to task relevant variables [29]. However, there has been a little work on examining the physical meanings of the muscle synergies extracted from EMGs. In addition, there has been a few trials to implement extracted synergies in robotic systems. A significant work is Artemiadis's *et al.* [36]. They extracted muscle synergies from EMG signals and applied them to a motor-driven manipulator. The large dimension of muscle-activation datasets was reduced into lower-dimensional motion primitives, which were then decoded back into high-dimensional joint space. This study would be useful for transferring human motions to a robot using movement profiles extracted from EMGs, but it did not address the stiffness information, another important aspect of motor control.

This dissertation consists of the following three main points:

1. Analysis of human muscle activities in a hand-force production task to identify muscle synergies. From the observed physical meanings of the extracted muscle synergies, we proposed a framework for neuro-mechanical control of the upper limb movements.

2. Design of a synergy control method for musculoskeletal robots based on the hypothesized framework and the analogy between human muscles and the pneumatic artificial muscles.

3. Role sharing between two human subjects in a crank-cooperation task. The role sharing was approached from the viewpoints of muscle synergies and kinematic.

How to extract and implement muscle synergies from EMGs based on the EP hypothesis is a key issue to deepen our understanding of the mechanism underlying motor control.

In our previous studies, we analyzed the surface EMG signals associated with human movements, such as hand-force control [17], walking [15], and running [43], based on the EP hypothesis. We extracted muscle synergies by defining the concept of the A-A ratio as the ratio of the EMGs of agonist and antagonist muscles. Note that this is different from the reciprocal command described by Feldman [5] in the framework of the EP hypothesis. The derivation of the A-A ratio and A-A activity concepts is based on the analogy between the biological system and a robot system with antagonistic artificial muscles. For biological muscles, the equilibrium length and stiffness of a muscle can be changed by the muscle activation [8]. Analogously, the natural length and elastic coefficient of an artificial muscle change according to the internal air pressure. The A-A ratio, defined as the ratio of the air pressure of the extensor artificial muscle and the sum of the air pressure of the extensor and flexor artificial muscles, is directly and linearly related to the equilibrium joint angle for a desired motion. The A-A activity, defined as the sum of the air pressure of the extensor and flexor artificial muscles, is directly and linearly associated with the joint stiffness at any equilibrium joint angle [47]. We expected that these concepts would be applicable to the biological system, providing variables to extract muscle synergies from EMG signals.

In this work, we provide a method to extract and implement muscle synergies from human EMGs to reproduce synergy commands that can be applied to pneumatic-driven robots to generate movements. To this purpose, we conducted a force-producing task experiment and examined the extracted muscle synergies with respect to the hand-forces generated. The number of synergies was chosen based on the number of principal components resulting from a principle component analysis (PCA) algorithm applied to the EMGs. In particular, two synergies were addressed. Using a linear regression analysis, we estimated the hand-force deviation in response to muscle synergies with the constraint that all muscle contractions were isometric. The regression results had a high coefficient of correlation,

emphasizing the high correlation between the extracted muscle synergies and the hand-forces. More importantly, the results led to the interpretation of the identified muscle synergies. Considering a polar coordinate frame centered on the shoulder joint, one synergy seemed to generate hand-forces in the angular direction, while the other synergy seemed to create hand-forces in the radial direction. Based on these results, we hypothesized a framework for motor control of the human upper limb. The framework suggests a simple and unique solution to combine multiple muscles generating muscle activities in order to produce desired movements.

From the outcomes of the human analysis, along with the proposed motor control framework, we devised a synergy-based control method for musculoskeletal robots whose joints are controlled by several pairs of pneumatic artificial muscles. The advantage of the method is that it employs a small number of variables to manipulate a number of joints. Instead of using a number of manipulated variables as other common control methods, this method uses only two synergies as manipulated variables to dealt with multiple degrees-of-freedom. Therefore, this method is suggestive for high-redundancy systems. To verify the efficacy of muscle synergies in motor control, we tested the synergy control method on a pneumatic-driven robotic arm whose structure mimicked the human arm's structure. The robotic arm had two links with three pneumatic artificial muscle pairs. The successful verification experiments proved the simplicity and efficacy of the synergy control method in making the robot generate movements properly as expected. This implementation would be useful for the developing neuro-rehabilitation assistance robots, as it satisfies a safety requirement that a neuro-rehabilitation assistance robot for the upper-limb motion should be capable of activating the arm movement gently and correctly.

Finally, we conducted experiments to observe the performance of two human subjects in a coordinated task. The observed role sharing would be helpful to improve the performance of musculoskeletal robots that involve in interaction tasks with human.

1.3 Organization of the entire dissertation

Chapter 2 presents the concepts of A-A ratio and A-A activity for artificial muscles and for human muscles. The physical meanings of the concepts are clarified. That is, the A-A ratio is directly and linearly related to the equilibrium joint angle for a desired motion. The A-A activity is directly and linearly associated with the joint stiffness at any equilibrium joint angle.

Chapter 3 exhibits the analysis of the human muscle activities in a hand-force production task. The technique to measure and to pre-process EMG signals is provided. Using A-A ratios, the physical meanings of the extracted muscle synergies can be elucidated. That is, considering a polar coordinate frame centered on the shoulder joint, one synergy seemed to generate hand-forces in the angular direction, while the other synergy seemed to create hand-forces in the radial direction. Based on the outcomes of the human muscle analysis, a novel framework for the motor control of the human upper limb movement is hypothesized. This framework suggests a simple and unique solution to combine multiple muscles, generating muscle activities in order to produce desired movements.

In Chapter 4, the synergy control method based on the proposed novel framework is demonstrated along with its verification implementation to a pneumatic-driven robotic arm.

Chapter 5 deals with the analysis of the dyad performance in a crank-cooperation task. Role divisions between the two dyad were observed, bringing suggestions to improve the performance of musculoskeletal robots that involve in interaction tasks with human.

Finally, Chapter 6 sums up the study and gives future plan.

CHAPTER II

A-A RATIO AND A-A ACTIVITY CONCEPTS

Based on the analogy between the human muscles and the artificial muscles, we devised the concepts of A-A ratio and A-A activity. At first, we investigated the characteristics of pneumatic artificial muscles (PAM) model and from that we proposed A-A ratio and A-A activity concepts. Then, we modified the concepts for human muscles.

2.1 A-A ratio and A-A activity for pneumatic artificial muscles

This section presents the derivation of A-A ratio and A-A activity concepts based on the investigations of the characteristics of PAM models. First, we present a single-joint model with one pair of PAMs to establish the basic characteristic of PAMs. Then, we expand the single-joint model with one pair of PAMs to a two-joint model with three pairs of PAMs.

2.1.1 A single-joint system with one pair of PAMs

In this section, we represent the characteristics of a PAM model based on the Fujimoto model [40]. The Fujimoto model, which was modified from the general PAM model proposed by Chou and Hannaford [6], is a linear approximation model of PAMs. It brings the advantage of a linear equation between the contraction force and the contraction ratio. It also addresses the account of energy loss.

Consider a PAM with the natural length L_0 [m]. Call P [Pa] the internal air pressure of PAM, F [N] the force produced by PAM, and L [m] the length of PAM. The contraction force can be expressed by the following linear equation

$$F = K(P)\{L - L_0(P)\}. \tag{1}$$

This equation indicates that a PAM can be modeled as a spring whose the elastic coefficient

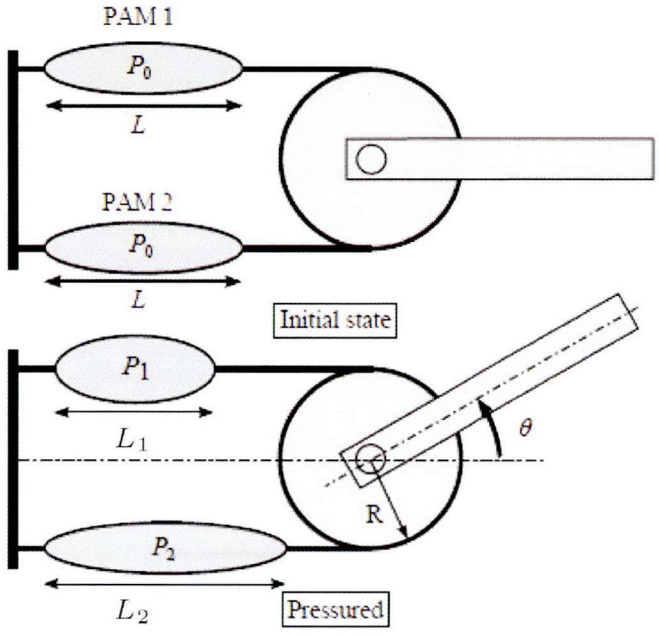

Figure 1: Sketch of a single-joint PAM model.

$K(P)$ and the natural length $L_0(P)$ change according to the internal air pressure P. These characteristics can be described as

$$K(P) = c_1 P + c_2, \tag{2}$$

$$L_0(P) = \frac{c_3}{K(P)} + c_4 \tag{3}$$

where c_i $(i = 1, 2, 3, 4)$ are property parameters of PAM. Equation (2) indicates that the elastic coefficient $K(P)$ increases as the internal air pressure P increases, while (3) indicates that the natural length $L_0(P)$ decreases as the internal air pressure P increases. Assuming that the internal pressure P is the command for muscle contraction, these characteristics of a PAM are analogous to those of a biological muscle [8].

Consider the single-joint model with one pair of PAMs as illustrated in Fig. 1. To investigate the physical properties of PAM1, we measured the changes in its length and contractile force according to the change in the internal pressure of PAM2. For more details, please see [47]. The system setup is illustrated in Fig. 2.

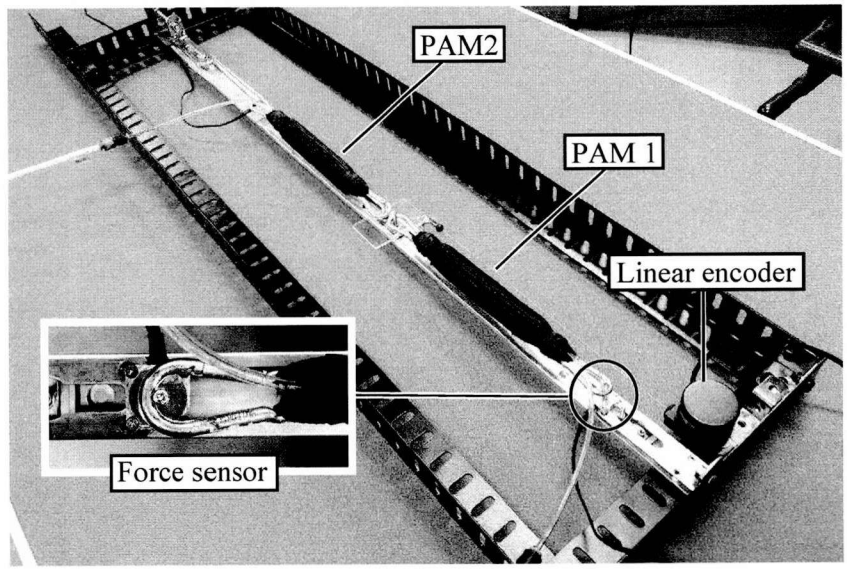

Figure 2: Experimental setup to identify PAM's properties. PAM's length was measured by a linear encoder; contractile force was measured by a force sensor.

2.1.1.1 A-A Ratio Concept

In the equilibrium state, the contraction forces of two PAMs balance each other, or

$$K(P_1)\{L_1 - L_0(P_1)\} = K(P_2)\{L_2 - L_0(P_2)\}. \tag{4}$$

The geometry constraint condition brings:

$$R\theta = L - L_1 = L_2 - L. \tag{5}$$

Equation (4) and (5) yield the joint angle θ:

$$\theta = \frac{L - c_4}{R} \cdot \frac{K(P_1) - K(P_2)}{K(P_1) + K(P_2)}. \tag{6}$$

Referring to (2) and constructing $\hat{P}_i = P_i - c_2/c_1$, $(i = 1, 2)$, we can rewrite $K(P_i)$ as

$$K(\hat{P}_i) = c_1\hat{P}_i. \tag{7}$$

The joint angle θ in (6) then can be expressed as

$$\theta = \frac{2(L - c_4)}{R} \cdot \left(\frac{\hat{P}_1}{\hat{P}_1 + \hat{P}_2} - \frac{1}{2}\right). \tag{8}$$

We define A-A ratio r as

$$r = \frac{\hat{P}_1}{\hat{P}_1 + \hat{P}_2}. \tag{9}$$

Substituting (9) into (8), a linear relationship between θ and r can be obtained,

$$\begin{aligned} \theta &= \frac{2(L - c_4)}{R}\left(r - \frac{1}{2}\right) \\ &= C\left(r - \frac{1}{2}\right) \end{aligned} \tag{10}$$

where $C = 2(L - c_4)/R$. As C is a constant, (10) indicates a linear relationship between the equilibrium angle θ and the A-A ratio r, bringing two advantages for controlling the antagonistic systems compared to other methods. First, it brings a unique solution of A-A ratio r according to the equilibrium angle θ although there are infinite candidates of PAM pressures that can achieve that condition. Second, it suggests a simple way to control joint movement by using the linear relationship between equilibrium angle θ and A-A ratio r.

2.1.1.2 A-A Activity Concept

A change of $\delta\theta$ results in a restoring force that drives the joint angle towards a new equilibrium angle θ. Let F_1' [N] and F_2' [N] be the forces generated by PAM1 and PAM2, respectively. F_1' and F_2' can be represented by the following two equations:

$$F_1' = F_1 - K(P_1)R\delta\theta, \tag{11}$$

$$F_2' = F_2 + K(P_2)R\delta\theta. \tag{12}$$

The restoring torque $\delta\tau$ [Nm] is

$$\begin{aligned} \delta\tau &= (F_2' - F_1')R \\ &= \{K(P_1) + K(P_2)\}R^2\delta\theta. \end{aligned} \tag{13}$$

From (7) and (13), we can derive the joint stiffness $G = d\tau/d\theta$ [Nm/rad] as

$$G = c_1R^2(\hat{P}_1 + \hat{P}_2). \tag{14}$$

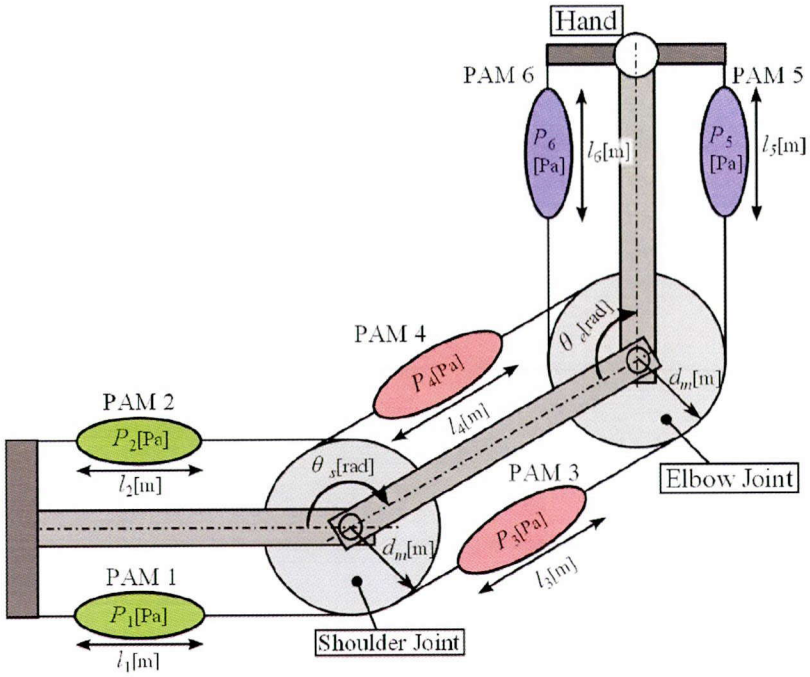

Figure 3: Sketch of the PAM model with two joints and six antagonistic muscles.

Defining A-A activity as

$$a = \hat{P}_1 + \hat{P}_2, \tag{15}$$

the stiffness G in (14) can be rewritten by

$$G = c_1 R^2 a. \tag{16}$$

This linear expression between the joint stiffness and A-A activity enables us to uniquely set the joint stiffness at any equilibrium angle and offers a simple control for the system.

2.1.2 A two-joint system with three pairs of PAMs

We expand the single-joint model with one pair of PAMs into a two-joint model with three pairs of PAMs. The PAM model mimics a human arm's structure with the shoulder and elbow joints and six antagonistic muscles around and connecting the two joints. The PAM model's structure and parameters are illustrated in Fig. 3. The six PAMs are labeled from PAM1 to PAM6. The names of the muscles corresponding to the six PAMs are listed in Table 1. Call P_i [Pa] the internal pressure of i-th PAM; l_i the length of i-th PAM; θ_s [rad]

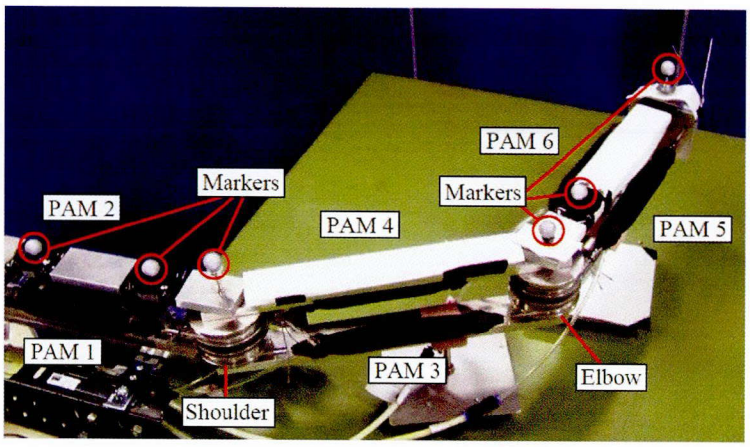

Figure 4: The experimental two-joint PAM model.

Table 1: PAMs and corresponding muscles.

PAM No.	Corresponding muscle
PAM1	Deltoid posterior
PAM2	Deltoid anterior
PAM3	Triceps long head
PAM4	Biceps
PAM5	Triceps lateral head
PAM6	Brachioradialis

and θ_e [rad] the shoulder- and elbow-joint angles; d_m the length of moment arm with the assumption that the moment arm of the shoulder joint and that of the elbow joint are equal. Figure 4 shows the experimental model.

In the equilibrium state, set $\theta_s = \theta_{s0}$, $\theta_e = \theta_{e0}$, $P_i = P_0$, and $l_i = L$. At this state, the contraction forces of the six PAMs balance each other, such that

$$F_1 - F_2 + F_3 - F_4 = 0;$$
$$F_3 - F_4 + F_5 - F_6 = 0. \tag{17}$$

Considering (1), we can rewritten (17) as

$$K(P_1)\{l_1 - l_0(P_1)\} - K(P_2)\{l_2 - l_0(P_2)\} + K(P_3)\{l_3 - l_0(P_3)\} - K(P_4)\{l_4 - l_0(P_4)\} = 0;$$
$$K(P_3)\{l_3 - l_0(P_3)\} - K(P_4)\{l_4 - l_0(P_4)\} + K(P_5)\{l_5 - l_0(P_5)\} - K(P_6)\{l_6 - l_0(P_6)\} = 0. \tag{18}$$

The geometry constraint condition brings

$$\begin{aligned} l_1 &= L - \mathrm{d_m}\delta\theta_s; \\ l_2 &= L + \mathrm{d_m}\delta\theta_s; \\ l_3 &= L - \mathrm{d_m}(\delta\theta_s + \delta\theta_e); \\ l_4 &= L + \mathrm{d_m}(\delta\theta_s + \delta\theta_e); \\ l_5 &= L - \mathrm{d_m}\delta\theta_e; \\ l_6 &= L + \mathrm{d_m}\delta\theta_e \end{aligned} \tag{19}$$

where $\delta\theta_s = \theta_s - \theta_{s0}$ and $\delta\theta_e = \theta_e - \theta_{e0}$ are deviations of the joint angles.

Given (3), substituting (19) into (18), we can obtain

$$\begin{bmatrix} K(P_1) + K(P_2) + K(P_3) + K(P_4) & K(P_3) + K(P_4) \\ K(P_3) + K(P_4) & K(P_3) + K(P_4) + K(P_5) + K(P_6) \end{bmatrix} \begin{bmatrix} \delta\theta_s \\ \delta\theta_e \end{bmatrix} = \frac{L - c_4}{\mathrm{d_m}} \begin{bmatrix} K(P_1) - K(P_2) + K(P_3) - K(P_4) \\ K(P_5) - K(P_6) + K(P_3) - K(P_4) \end{bmatrix}. \tag{20}$$

Given (7), the deviations of joint angles $\delta\boldsymbol{\theta} = \left[\delta\theta_s, \delta\theta_e\right]^T$ in (20) then can be expressed as

$$\delta\boldsymbol{\theta} = \frac{2(L - c_4)}{\mathrm{d_m}} \begin{bmatrix} \hat{a}_{11} & \hat{a}_{12} & \hat{a}_{13} \\ \hat{a}_{21} & \hat{a}_{22} & \hat{a}_{23} \end{bmatrix} \tag{21}$$

where

$$\hat{a}_{11} = \frac{(\hat{P}_1 + \hat{P}_2)(\hat{P}_3 + \hat{P}_4 + \hat{P}_5 + \hat{P}_6)(\frac{\hat{P}_1}{\hat{P}_1+\hat{P}_2} - 0.5)}{(\hat{P}_1 + \hat{P}_2)(\hat{P}_3 + \hat{P}_4) + (\hat{P}_3 + \hat{P}_4)(\hat{P}_5 + \hat{P}_6) + (\hat{P}_5 + \hat{P}_6)(\hat{P}_1 + \hat{P}_2)};$$

$$\hat{a}_{12} = \frac{(\hat{P}_3 + \hat{P}_4)(\hat{P}_5 + \hat{P}_6)(\frac{\hat{P}_3}{\hat{P}_3+\hat{P}_4} - 0.5)}{(\hat{P}_1 + \hat{P}_2)(\hat{P}_3 + \hat{P}_4) + (\hat{P}_3 + \hat{P}_4)(\hat{P}_5 + \hat{P}_6) + (\hat{P}_5 + \hat{P}_6)(\hat{P}_1 + \hat{P}_2)};$$

$$\hat{a}_{13} = \frac{-(\hat{P}_3 + \hat{P}_4)(\hat{P}_5 + \hat{P}_6)(\frac{\hat{P}_5}{\hat{P}_5+\hat{P}_6} - 0.5)}{(\hat{P}_1 + \hat{P}_2)(\hat{P}_3 + \hat{P}_4) + (\hat{P}_3 + \hat{P}_4)(\hat{P}_5 + \hat{P}_6) + (\hat{P}_5 + \hat{P}_6)(\hat{P}_1 + \hat{P}_2)};$$

$$\hat{a}_{21} = \frac{-(\hat{P}_1 + \hat{P}_2)(\hat{P}_3 + \hat{P}_4)(\frac{\hat{P}_1}{\hat{P}_1+\hat{P}_2} - 0.5)}{(\hat{P}_1 + \hat{P}_2)(\hat{P}_3 + \hat{P}_4) + (\hat{P}_3 + \hat{P}_4)(\hat{P}_5 + \hat{P}_6) + (\hat{P}_5 + \hat{P}_6)(\hat{P}_1 + \hat{P}_2)};$$

$$\hat{a}_{22} = \frac{(\hat{P}_1 + \hat{P}_2)(\hat{P}_3 + \hat{P}_4)(\frac{\hat{P}_3}{\hat{P}_3+\hat{P}_4} - 0.5)}{(\hat{P}_1 + \hat{P}_2)(\hat{P}_3 + \hat{P}_4) + (\hat{P}_3 + \hat{P}_4)(\hat{P}_5 + \hat{P}_6) + (\hat{P}_5 + \hat{P}_6)(\hat{P}_1 + \hat{P}_2)};$$

$$\hat{a}_{23} = \frac{(\hat{P}_5 + \hat{P}_6)(\hat{P}_1 + \hat{P}_2 + \hat{P}_3 + \hat{P}_4)(\frac{\hat{P}_5}{\hat{P}_5+\hat{P}_6} - 0.5)}{(\hat{P}_1 + \hat{P}_2)(\hat{P}_3 + \hat{P}_4) + (\hat{P}_3 + \hat{P}_4)(\hat{P}_5 + \hat{P}_6) + (\hat{P}_5 + \hat{P}_6)(\hat{P}_1 + \hat{P}_2)}.$$

From (9) and (15) we have the A-A ratio and A-A activity for each PAM pair as

$$r_i = \frac{\hat{P}_{2i-1}}{\hat{P}_{2i-1} + \hat{P}_{2i}}, \tag{22}$$

$$a_i = \hat{P}_{2i-1} + \hat{P}_{2i}; \tag{23}$$

where i indicates the PAM pair index ($i = 1, 2, 3$). Setting the ratio deviation $\delta r_i = r_i - 0.5$, the deviations of joint angles $\delta\boldsymbol{\theta}$ in (21) can be rewritten as

$$\begin{aligned}\delta\boldsymbol{\theta} &= \frac{2(L - c_4)}{\mathrm{d_m}} \begin{bmatrix} \frac{a_1a_2+a_1a_3}{a_1a_2+a_2a_3+a_1a_3} & \frac{a_2a_3}{a_1a_2+a_2a_3+a_1a_3} & \frac{-a_2a_3}{a_1a_2+a_2a_3+a_1a_3} \\ \frac{-a_1a_2}{a_1a_2+a_2a_3+a_1a_3} & \frac{a_1a_2}{a_1a_2+a_2a_3+a_1a_3} & \frac{a_1a_3+a_2a_3}{a_1a_2+a_2a_3+a_1a_3} \end{bmatrix} \begin{bmatrix} \delta r_1 \\ \delta r_2 \\ \delta r_3 \end{bmatrix} \\ &= \mathbf{A}\delta\mathbf{r}\end{aligned} \tag{24}$$

where

$$\mathbf{A} = \frac{2(L - c_4)}{\mathrm{d_m}} \begin{bmatrix} \frac{a_1a_2+a_1a_3}{a_1a_2+a_2a_3+a_1a_3} & \frac{a_2a_3}{a_1a_2+a_2a_3+a_1a_3} & \frac{-a_2a_3}{a_1a_2+a_2a_3+a_1a_3} \\ \frac{-a_1a_2}{a_1a_2+a_2a_3+a_1a_3} & \frac{a_1a_2}{a_1a_2+a_2a_3+a_1a_3} & \frac{a_1a_3+a_2a_3}{a_1a_2+a_2a_3+a_1a_3} \end{bmatrix};$$

$$\delta\mathbf{r} = \begin{bmatrix} \delta r_1, \delta r_2, \delta r_3 \end{bmatrix}^T.$$

Table 2: Definition of A-A Ratio and A-A activity.

Ratio	Physical property
$r_1 = m_1/(m_1 + m_2)$	Shoulder extension
$r_2 = m_3/(m_3 + m_4)$	(Shoulder) elbow extension
$r_3 = m_5/(m_5 + m_6)$	Elbow extension
$r_4 = m_7/(m_7 + m_8)$	(Elbow) wrist extension
Activity	**Physical property**
$a_1 = m_1 + m_2$	Shoulder joint stiffness
$a_2 = m_3 + m_4$	(Shoulder) elbow joint stiffness
$a_3 = m_5 + m_6$	Elbow joint stiffness
$a_4 = m_7 + m_8$	(Elbow) wrist joint stiffness

This equation indicates that if $\{a_1, a_2, a_3\}$ are constant, the relationship between $\delta\boldsymbol{\theta}$ and $\delta\mathbf{r}$ is linear, thus, suggesting a simple way to control the system that replicates the human arm with two joints and three pairs of antagonistic muscles around and connecting the joints.

2.2 A-A ratio and A-A activity for the human muscles

For PAM systems, we defined A-A ratio and A-A activity with respect to the pressures supplied to each PAM as in (22) and (23), respectively. To apply these definitions to the human muscles, we selected the antagonistic muscle pairs from anatomical point of view and modified them with respect to the EMGs of each muscle. The A-A ratio and A-A activity are respectively defined by

$$r_i = \frac{m_{2i-1}}{m_{2i-1} + m_{2i}},$$
$$a_i = m_{2i-1} + m_{2i} \tag{25}$$

where i indicates the i-th muscle pair. Here, we examined four pairs of antagonistic muscles that mainly contributed to the studied task, or ($i = 1, 2, 3, 4$). Physical properties of A-A ratio and A-A activity of the four examined muscle pairs are given in Table 2.

By defining A-A ratio as in (25), we can explain the kinematic of joint movement. For example, the kinematic of the shoulder joint can be elaborated by the change in A-A

ratio $r_1 = m_1/(m_1 + m_2)$. When m_1 increases and m_2 decreases or m_1 is greater than m_2, the A-A ratio r_1 increases. Because the extensor muscle m_1 works harder than the flexor muscle m_2, the shoulder joint will extend. Hence, a change in the A-A ratio r_1 will relate to the kinematic of the shoulder-joint movement. This mechanism can be elucidated by a linear relationship between A-A ratio and joint angle which was reported in the case of musculoskeletal robots built with pneumatic-artificial muscles [48]. The linear relationship between the A-A ratio and the equilibrium state [47] also supports for the physical meaning of the proposed A-A ratio. That is, when the agonist and antagonist muscles contract unequally, or the A-A ratio varies, joint movement will be generated, driving the system to a new equilibrium-joint angle. In addition, the linear relationship between the A-A ratio and the equilibrium-joint angle also offers a simple way to control the joint movement.

On the other hand, as the stiffness of a muscle is proportional to its level of activity [45], the joint stiffness is proportional to the sum of the activity level of agonist and antagonist muscles across the joint. Therefore, by defining an A-A activity as the sum of the EMGs of an antagonistic muscle pair, we can explain the contribution of each muscle pair to the joint stiffness. For example, when both muscles m_1 and m_2 contract or m_1 and m_2 increase, the A-A activity $a_1 = m_1 + m_2$ will increase. Physiologically, the contraction of these two muscles results in an increase of the shoulder-joint stiffness. Hence, the A-A activity a_1 is related to the shoulder-joint stiffness. This relationship between the A-A activity and the joint stiffness was also experimentally proved in [47].

In short, using the proposed A-A ratio and A-A activity, we expected to easily and separately control the equilibrium joint angle and the joint stiffness, which, consequently, generates arm movements. This separate control was evidenced for the motor cortex of the monkey [10]. When stimulating one neuron group, the joint movement was generated; when stimulating the other neuron group, the muscle co-contraction was activated.

CHAPTER III

EXTRACTION AND IMPLEMENTATION OF MUSCLE SYNERGIES IN HAND-FORCE CONTROL

3.1 Introduction

The need of solving the problem of multi-degrees-of-freedom in motor control is increasing as human-like robots become more popular these days. Muscle synergies hypothesis is a prominent suggestion for this problem. This chapter presents an investigation of the muscle synergies extracted from human subjects in a hand-force production task to explore the mechanism of the human's skillful hand-movement at producing force while manipulating objects. We observed a high correlation estimation of the muscle synergies with the hand-force, and derived a role division of muscle synergies in generating the hand-force as well. These results give an optimal but simple way to control robots so as to make the robots' movement as skillful as human's.

Recent research have focused on the muscle activation characters of the human hand, a high degree-of-freedom structure. Levin [35] tried to establish the patterns of muscle activation in association with movement orientation. They cited an insufficient explanation of how the CNS manages muscle groups to produce limb movements. This matter is likely solved by concerning the muscle synergies hypothesis. That is, the CNS controls hand movements by using muscle synergies to reduce the dimensionality of the multiple-dimensional structure; the control, therefore, becomes simpler and easier. d'Avella [1] investigated extracted muscle synergies in point-to-point movement in different conditions. They reported that, given a set of synergies, the time-varying model can describe muscle

patterns parsimoniously. All characteristics of each individual muscle activity are organized into muscle synergies, hence, characteristics of muscle pattern for reaching can be the results of the combination of a few muscle synergies. Turner [9] explored the direction-dependent muscle synergy behavior at different arm joints during reaching movements. They discussed that a range of muscle activation synergies in healthy subjects can enable precise and well timed reaching movements in different direction with robot-induced force fields. This suggests that muscle groups can act in a modular fashion. However, no clear interpretation of the meanings of muscle synergies has been approached. In addition, there has been a little work that tried to implement extracted synergies in robotic systems. Artemiadis presented a human-machine interface using EMGs [36]. However, they did not discuss the stiffness control. Motivated by these research, we investigated the correlation between muscle activities and hand movements, and the role of muscle synergies in generating hand-forces, by focusing on muscle activities and its output, the hand-force vector, instead of the muscle force as they are task-relevant variables. Assuming that all muscle contractions are isometric, we examined the regression model for the hand-force deviation bearing on muscle activities, and explored muscle force synergies. Using A-A ratios, we can investigate the physical meanings of the extracted muscle synergies.

3.2 Materials and methods

3.2.1 The task

The aim of this experiment is to investigate the properties of muscle activities in generating the hand-forces in an isometric condition. To this aim, we measured EMGs and hand-forces in an isolated movement and examined the relationship between them. Subjects were asked to produce 8 N of force pointing along eight directions in a horizontal plane, starting at direction 1 and shifting orientation by 45° in the counterclockwise rotation until ending at direction 8 (see Fig. 5). The task goal was to produce a hand-force as

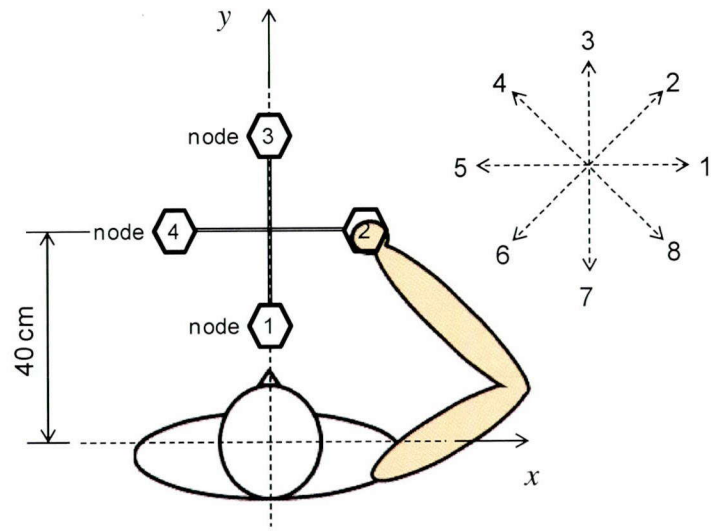

Figure 5: Experimental setup, top view. Subjects were asked to produce force along eight directions in order, from direction 1 to direction 8. The task was performed with each arm, and it was identical for both arms.

close to the reference force as possible and to keep maintaining the force in a 6-second duration before producing a hand-force into the next direction. The task was performed with the left hand and the right hand, and it was identical for both hands. Subjects performed the task at four different arm postures (at node 1, node 2, node 3, and node 4).

3.2.2 Subjects

Three healthy volunteers (22 years old, healthy male, right-handed) with no record of neuromuscular deficits participated in the experiment. The experiment procedures were conducted with the approval of the Ethics Committee, Osaka University.

3.2.3 Experimental setup

Subjects sat comfortably on chairs, with the elbow lifted by a string to reduce the gravitational effect and to allow the shoulder and elbow flexion-extension in a horizontal plane. Subjects grasped the joystick and pulled or pushed it to produce hand-forces at a comfortable speed while looking at reference forces displayed on a screen. For analysis simplicity, the wrist movement was prevented by a splint so that it could be ignored. The posture was

considered regarding to [34] to examine the characteristics of single-joint and two-joint muscles in producing the hand-forces. EMGs of eight muscles (see Fig. 6) which mainly contribute to the studied task were collected by using multi-telemeter system (WEB-5000, Nihon Kohden) at 1000 Hz. A force sensor (USL06-H5-200, TecGihan) was attached under the joystick to measure the hand-forces. For every trial, the EMGs and hand-forces were synchronized and collected at a sampling rate of 1000 Hz.

EMGs measurement

Electromyograms are electrical activities of muscles. Recording and evaluating electromyograms is a technique called electromyography (EMG). Recently, EMGs are the common tool to investigate muscle activities. EMGs are also the control interfaces for robotic devices. Investigating the EMGs of the human muscles, we can directly clarify the characteristics of muscle activities or the input of movements. However, EMGs contain a lot of noises so the measurement and processing should be carried out with much care. In the following, we present the procedure to collect EMG signals.

EMG signals of examined muscles were collected by using multi-telemeter systems (WEB-5000, Nihon Kohden) at 1000 Hz. We examined eight antagonistic muscles of the upper limb that mainly contribute to the studied movements in a horizontal plane. Examined muscles (see Fig. 6) were identified according to the guidelines in [16]. First, the skin was cleaned to reduce the resistance below 10 kΩ. Then, surface electrodes were placed on the examined muscles. Figure 7 illustrates the placement of surface electrodes on the examined muscles. The distance between two electrodes was 2 centimeters. EMG signals were band-pass filtered (0.03 to 450 Hz), hum filtered (60 Hz), amplified (x2000), and stored in a computer.

Initially, the Maximum Voluntary Contraction (MVC) or the maximum value of EMGs of subjects' muscles were measured. The subjects then practiced the task several times to get familiar with the system and the task goal. After practicing, subjects performed the experiment trials.

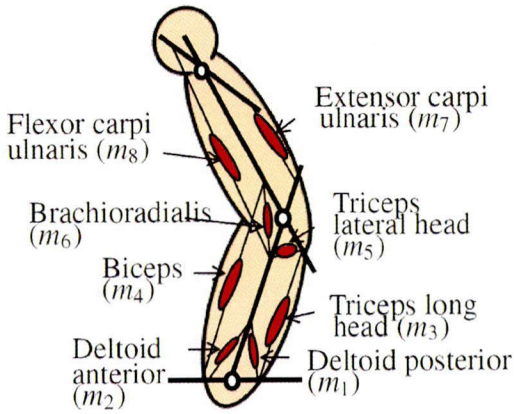

Figure 6: Sketch of examined muscles which mainly contribute to the studied movement in the horizontal plane.

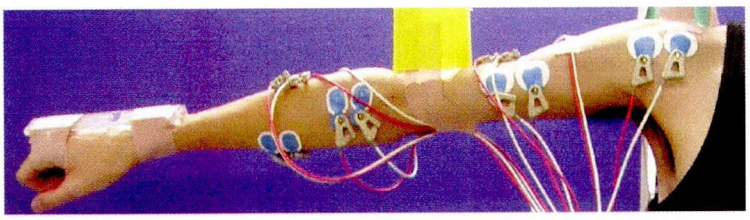

Figure 7: Illustration of the placement of electrodes on examined muscles of subjects.

3.2.4 Data processing

3.2.4.1 EMG pre-processing

The raw EMG signals, which contain many noises and artifacts, need to be pre-processed to become more reliable for the analysis. The process includes:

1. Band-pass filter (10-450 Hz) the raw EMGs to reduce anti-aliasing effects within sampling.

2. Full-wave rectify EMGs to make them more readable.

3. Smooth EMGs by a low-pass filter (5 Hz).

4. Amplitude normalize the signals to MVC so as to eliminate the influence of the

detection condition and to make the data comparable between different muscles as well as between different subjects.

3.2.4.2 *Data normalizing*

The dataset of EMGs in each trial is a $n \times 8$ matrix:

$$\mathbf{m}(t) = \begin{bmatrix} m_1(t_1) & m_2(t_1) & \cdots & m_8(t_1) \\ \vdots & \vdots & \vdots & \vdots \\ m_1(t_n) & m_2(t_n) & \cdots & m_8(t_n) \end{bmatrix} \tag{26}$$

where $m_i(t)$ is the time-varying EMG signal of i-th muscle at time t; and n indicates the time points in a trial. To observe the whole process of generating movements in each trial, the EMG signals are averaged with respect to time. The dataset of the averaged EMGs in a trial is a 8×8 matrix corresponding to the eight directions:

$$\mathbf{m}(k) = \begin{bmatrix} m_1(k_1) & m_2(k_1) & \cdots & m_8(k_1) \\ \vdots & \vdots & \vdots & \vdots \\ m_1(k_n) & m_2(k_n) & \cdots & m_8(k_n) \end{bmatrix} \tag{27}$$

where k indicates the direction. Here, since the task was to produce hand-forces into eight directions, $(k = 1, 2, \cdots, 8)$. In addition, we standardized the EMGs as follows

$$m(k) = \frac{m^\star(k)}{\sqrt{\sum_{k=1}^{8}(m^\star(k) - \overline{m^\star})^2}} \tag{28}$$

where $m^\star(k)$ is the averaged EMG of a muscle at k-th direction $(k = 1, 2, \cdots, 8)$ and $\overline{m^\star}$ is the average of $m^\star(k)$ over all directions.

The hand-force data are also averaged with respect to time. The dataset of hand-forces (F_x, F_y) in a trial is a 8×2 matrix corresponding to the eight directions ks:

$$\mathbf{F}(k) = \begin{bmatrix} F_x(k_1) & F_y(k_1) \\ \vdots & \vdots \\ F_x(k_8) & F_y(k_8) \end{bmatrix}. \tag{29}$$

3.2.5 A-A ratio and A-A activity datasets

In Chapter 2, we proposed the definitions of A-A ratio and A-A activity for the human muscles as in (25):

$$r_i = \frac{m_{2i-1}}{m_{2i-1} + m_{2i}},$$
$$a_i = m_{2i-1} + m_{2i}$$

where i indicates the i-th muscle pair.

A-A ratio of the data in (27) with the EMGs $m(k)$ defined as in (28) then can be expressed as a 8×4 matrix corresponding to the eight directions

$$\mathbf{r}(k) = \begin{bmatrix} r_1(k_1) & r_2(k_1) & r_3(k_1) & r_4(k_1) \\ \vdots & \vdots & \vdots & \vdots \\ r_1(k_n) & r_2(k_n) & r_3(k_n) & r_4(k_n) \end{bmatrix}. \tag{30}$$

A-A activity of the data in (27) with the EMGs $m(k)$ defined as in (28) is a 8×4 matrix corresponding to the eight directions

$$\mathbf{a}(k) = \begin{bmatrix} a_1(k_1) & a_2(k_1) & a_3(k_1) & a_4(k_1) \\ \vdots & \vdots & \vdots & \vdots \\ a_1(k_n) & a_2(k_n) & a_3(k_n) & a_4(k_n) \end{bmatrix}. \tag{31}$$

Now we present the way to reduce the dimension of the A-A ratio and A-A activity dataset. A widely used statistical technique for reducing the data dimensionality is the principal component analysis (PCA) [18]. For example, Artemiadis *et al.* [36] embedded the high-dimensional dataset of muscle activations and corresponding joint angles into two manifolds of fewer dimensions. This reduction has two advantages. For joint angles, using fewer variables to describe movement suggests motor primitives. For analysis reasons, it is attractive to represent back the two manifolds into the high-dimensional space. Therefore, it is suggestive that applying PCA to the datasets of the A-A ratio we can find a new representation for these data and can represent the arm motion in the Cartesian space by

Table 3: Percentage of variation accounted for by the first two PCs.

Node	Subject	Right hand			Left hand		
		PC1	PC2	Total	PC1	PC2	Total
1	A	81.27	16.53	97.80	69.35	29.84	99.19
	B	65.14	29.70	94.84	71.55	25.97	97.52
	C	66.42	30.77	97.19	49.99	45.47	95.46
2	A	74.65	20.58	95.23	72.05	25.81	97.87
	B	67.85	29.51	97.36	74.05	24.76	98.81
	C	63.79	33.37	97.16	50.95	37.22	88.17
3	A	77.47	20.56	98.03	88.45	10.63	99.08
	B	73.71	24.91	98.62	60.13	34.98	95.11
	C	62.61	32.70	95.31	62.53	30.23	92.76
4	A	83.23	14.34	97.57	67.84	29.97	97.81
	B	61.79	34.54	96.33	68.30	28.34	96.64
	C	57.69	33.85	91.54	68.86	26.58	95.44

using fewer independent variables. For example, the A-A ratios can be represented by a linear combination as

$$\delta \mathbf{r} = \sum_{i=1}^{4} w_i(k)\mathbf{s}_i \tag{32}$$

where $\delta \mathbf{r} = \mathbf{r}(k) - \mathbf{r}_0$, with $\mathbf{r}_0$ is the averaged value of $\mathbf{r}(k)$ in all directions; $w_i(k)$ and $\mathbf{s}_i$ are the i-th principal component score and the i-th principal component vector, respectively. Principal components (PC) are found from covariance matrix.

3.3 *Results and discussion*

3.3.1 EMGs reducing

The number of PCs retained was chosen so as to preserve the most information of EMGs. For this task, the first two PCs of the A-A ratios contributed over 90% of the total variation of the A-A ratios (see Table 3). Therefore, the A-A ratio data can be reasonably represented by the first two PCs. Here, we present the analysis results of only one subject (subject A) as the obtained results were consistent across all of the subjects.

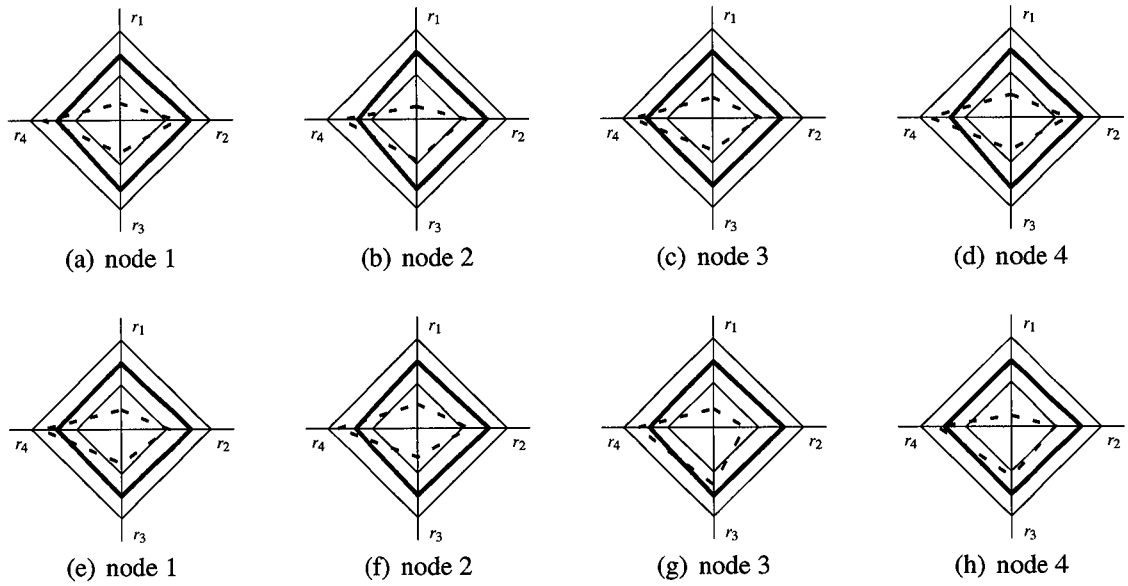

Figure 8: PC vectors resulting from PCA algorithm of left hand (upper row) and right hand (lower row). Thick solid lines: PC1 vectors; dashed lines: PC2 vectors. All thick-solid-line quadrangles (PC1 vectors) stretched uniformly into four edges, and located between the outer and inner squares; dashed-line quadrangles (PC2 vectors) seem to be stretched horizontally.

3.3.2 PC vectors

A correspondence between PC vectors resulting from PCA of the left hand and those of the right hand was observed. Figure 8 shows the PC vectors of the left hand (upper row) and those of the right hand (lower row). Thick solid lines represent for PC1 vectors; dashed lines represent for PC2 vectors. In each graph, the outer square is level 1, the inner square is level 0, and the center is level -1. Axes $\{r_1, r_2, r_3, r_4\}$ indicates the value of the element corresponding to $\{r_1, r_2, r_3, r_4\}$, respectively; thus, the horizontal axis accords with two-joint muscle activities while the vertical axis conforms to one-joint muscle activities. Each element of the PC vectors is within the range of [-1,1]. As seen in this figure, plot of PC vectors of the left hand and that of the right hand are almost the same shape at symmetric positions (at node 1 for both hands, at node 2 for the left hand and node 4 for the right hand, at node 4 for the left hand and node 2 for the right hand, and slightly different at node 3). A symmetry between the PC vectors of the left hand and those of the right hand, hence, can be

concluded. They are similar when the left and right arm postures are symmetric. Besides, the PC1 vectors are all located uniformly between the outer and inner squares while the PC2 vector shapes seem to be horizontally stretched, suggesting that the first vector was generated by all the muscles at a same level whereas one-joint muscles took the major role in generating the PC2 vector. This result gives a practical idea of using PC vectors in the robot control.

Moreover, PC vectors indicate muscles' combinations. For PC1 vectors, all the elements are positive. For PC2 vectors, the element corresponding to r_1 is negative; the element relating to r_4 is positive; and the remaining two elements are approximate 0. The even location of the elements of PC1 vectors on all the axes implies a similar contribution of all muscle extension, whereas the distribution of PC2 vector elements, weighting to r_1 and r_4, infers a simultaneous contribution of the shoulder flexion and elbow extension. PC vectors, therefore, can also be considered as the representation of synergies that merge the coordination of multi-articular muscles [31]. Particularly, in case of the hand-force generation task, any force vector in a horizontal plane can be generated by two synergies. Muscle synergies, which are commonly difficult to understand from the original EMGs, becomes interpretable when being represented by PC vectors derived from A-A ratios of the original EMGs. In other words, by using PC vectors we can clarify the physical meanings of muscle synergies more clearly. This characteristic will be discussed in detail in the next section.

3.3.3 PC scores

Figure 9 plots the hand-forces and the scores of the first two PCs (trial at node 1). The left column presents the observations of hand-force deviation (F_x, F_y); the right column indicates the PC scores (w_1, w_2). The top row is the result of the left-hand test; the bottom row is the result of the right-hand test. As seen in this figure, the PC scores all go around a central point, just like the generated hand-forces. Each observation (Obs) corresponds to one force direction (Dirn). Arrows represent for the observations from direction 1 to

direction 8. There is nearly a symmetry between the PC scores of the left hand and those of the right hand; for example, PC scores for direction 1 (Obs 1) of the left-hand trial are about the same as those for direction 5 (Obs 5) of the right-hand trial; only Obs 5 for the left-hand trial and Obs 1 for the right-hand trial are vaguely symmetric. The correspondence is summarized as in Table 4. Since the shape of PC scores resembles the circle-like shape of the hand-forces, it is expected a high correlation between PC scores and the hand-forces.

Moreover, the PC scores of the right hand are almost the same as those of the left hand at symmetric positions, reflecting the fact that the right and left arm postures are symmetric (see Fig. 10 and 11). These facts suggest an interesting aspect of bimanual movements, that is, it is easy for us to make simultaneous movements of the hands if the patterns for the two hands are mirror images of each other [38].

Table 4: Correspondence between left-hand test and right-hand test.

	Corresponding positions							
Left-hand test	1	2	3	4	5	6	7	8
Right-hand test	5	4	3	2	1	8	7	6

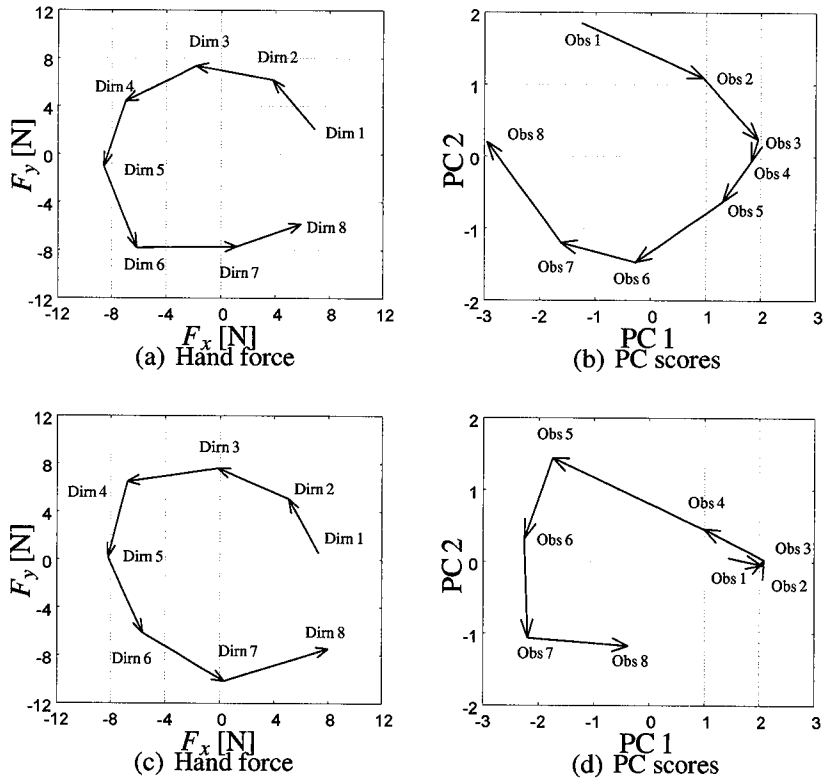

Figure 9: Observations of hand-force and PC scores corresponding to force vectors at node 1 for the left-hand trial (upper row) and the right-hand trial (lower row). Plots of PC scores almost resemble the shape of hand-force. Plots of PC scores of the left-hand trial and those of the right-hand trial are about the same due to a physical symmetry.

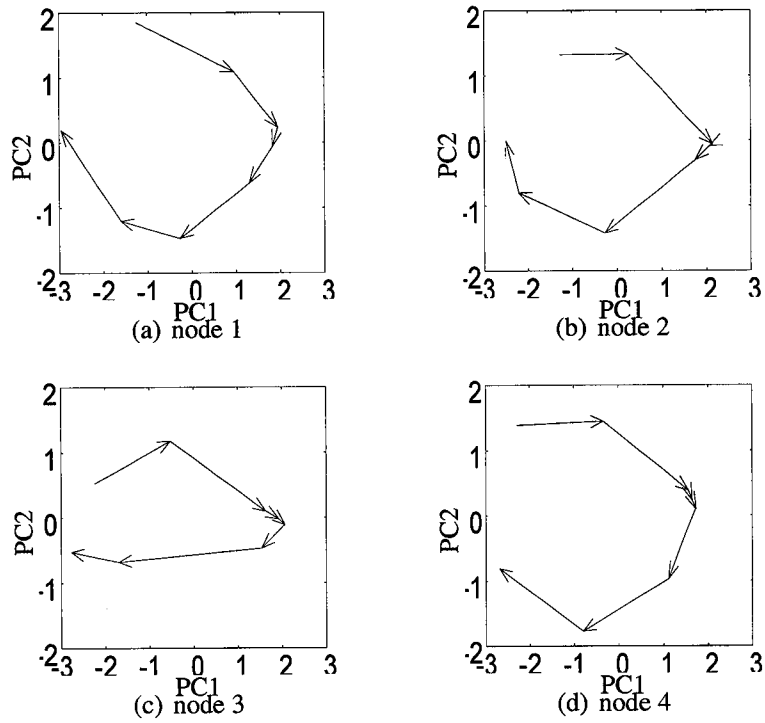

Figure 10: PC scores of left hand.

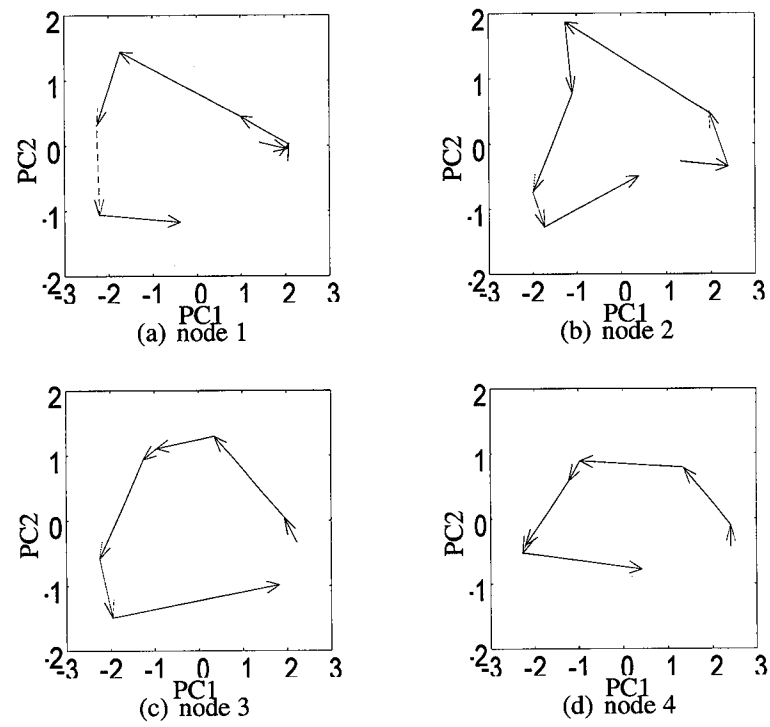

Figure 11: PC scores of right hand.

3.3.4 Hand-force estimation

Here, we assume that hand-forces are generated by manipulating the equilibrium joint angle defined as A-A ratio. Let $\delta\boldsymbol{\theta}$ be a deviation of the equilibrium joint angular vector giving joint torques $\boldsymbol{\tau}$ as a result of the joint stiffness such that

$$\boldsymbol{\tau} = \mathbf{K}\delta\boldsymbol{\theta} \tag{33}$$

where $\mathbf{K}$ is a joint stiffness matrix. Moreover, since the hand-force can be converted into the equivalent joint torques according to the relationship $\boldsymbol{\tau} = \mathbf{J}^T\mathbf{F}$ where $\mathbf{J}^T$ is the transpose of the Jacobian which represents the infinitesimal relationship between the joint displacements and the hand position, the hand-force is determined by the following linear equation

$$\mathbf{F} = (\mathbf{J}^T)^{-1}\mathbf{K}\delta\boldsymbol{\theta}, \tag{34}$$

provided that the Jacobian is non-singular. Considering the linear relationship $\delta\boldsymbol{\theta} = \mathbf{A}\delta\mathbf{r}$ in (24), we obtain

$$\mathbf{F} = (\mathbf{J}^T)^{-1}\mathbf{K}\mathbf{A}\delta\mathbf{r}, \tag{35}$$

which means that the hand-force can be controlled by A-A ratio.

Also worth noting is that the A-A ratio data can be approximately represented by the first two PCs of the A-A ratio as

$$\delta\mathbf{r}(k) \fallingdotseq w_1(k)\mathbf{s}_1 + w_2(k)\mathbf{s}_2 \tag{36}$$

where $\mathbf{s}_1$ and $\mathbf{s}_2$ represent muscle synergies in terms of A-A ratio $\mathbf{r}$. Then (35) yields the following relationship between the hand-force and PC vectors

$$\begin{aligned}\mathbf{F}(k) &\fallingdotseq w_1(k)\mathbf{Q}\mathbf{s}_1 + w_2(k)\mathbf{Q}\mathbf{s}_2 \\ &= w_1(k)\mathbf{p}_1 + w_2(k)\mathbf{p}_2\end{aligned} \tag{37}$$

where $\mathbf{Q} = (\mathbf{J}^T)^{-1}\mathbf{K}\mathbf{A}$ is a linear mapping operator onto the hand-force vector space, and $\mathbf{p}_1 = \mathbf{Q}\mathbf{s}_1$ and $\mathbf{p}_2 = \mathbf{Q}\mathbf{s}_2$ are muscle synergies represented in terms of the hand-force vector.

Table 5: Regression model for hand-force by PC scores (left hand).

Node	R^2 for F_x	R^2 for F_y	Regression model
1	0.86	0.95	$\begin{pmatrix}\Delta\mathbf{F}_x\\ \Delta\mathbf{F}_y\end{pmatrix} = \begin{pmatrix}-2.20\\ 2.47\end{pmatrix}\mathbf{w}_1 + \begin{pmatrix}3.59\\ 3.71\end{pmatrix}\mathbf{w}_2$
2	0.87	0.92	$\begin{pmatrix}\Delta\mathbf{F}_x\\ \Delta\mathbf{F}_y\end{pmatrix} = \begin{pmatrix}-2.21\\ 2.62\end{pmatrix}\mathbf{w}_1 + \begin{pmatrix}5.1\\ 4.22\end{pmatrix}\mathbf{w}_2$
3	0.93	0.67	$\begin{pmatrix}\Delta\mathbf{F}_x\\ \Delta\mathbf{F}_y\end{pmatrix} = \begin{pmatrix}-2.44\\ 1.17\end{pmatrix}\mathbf{w}_1 + \begin{pmatrix}4.3\\ 7.35\end{pmatrix}\mathbf{w}_2$
4	0.87	0.80	$\begin{pmatrix}\Delta\mathbf{F}_x\\ \Delta\mathbf{F}_y\end{pmatrix} = \begin{pmatrix}-2.93\\ 1.47\end{pmatrix}\mathbf{w}_1 + \begin{pmatrix}2.24\\ 4.66\end{pmatrix}\mathbf{w}_2$

Table 6: Regression model for hand-force by PC scores (right hand).

Node	R^2 for F_x	R^2 for F_y	Regression model
1	0.69	0.93	$\begin{pmatrix}\Delta\mathbf{F}_x\\ \Delta\mathbf{F}_y\end{pmatrix} = \begin{pmatrix}1.51\\ 2.92\end{pmatrix}\mathbf{w}_1 + \begin{pmatrix}-5.36\\ 4.22\end{pmatrix}\mathbf{w}_2$
2	0.71	0.84	$\begin{pmatrix}\Delta\mathbf{F}_x\\ \Delta\mathbf{F}_y\end{pmatrix} = \begin{pmatrix}2.15\\ 1.91\end{pmatrix}\mathbf{w}_1 + \begin{pmatrix}-1.90\\ 4.74\end{pmatrix}\mathbf{w}_2$
3	0.98	0.89	$\begin{pmatrix}\Delta\mathbf{F}_x\\ \Delta\mathbf{F}_y\end{pmatrix} = \begin{pmatrix}2.15\\ 1.24\end{pmatrix}\mathbf{w}_1 + \begin{pmatrix}-1.83\\ 4.67\end{pmatrix}\mathbf{w}_2$
4	0.88	0.96	$\begin{pmatrix}\Delta\mathbf{F}_x\\ \Delta\mathbf{F}_y\end{pmatrix} = \begin{pmatrix}1.80\\ 1.85\end{pmatrix}\mathbf{w}_1 + \begin{pmatrix}-4.42\\ 46.67\end{pmatrix}\mathbf{w}_2$

In the following, we call $(\mathbf{p}_1, \mathbf{p}_2)$ synergy force vectors. Synergy force vectors can be estimated by the linear regression model of (37).

As indicated in Table 5 and 6, in most cases, this model can explain approximately more than 80% of the variation in the hand-force profiles (the regression coefficient, R^2, exceeds 80% for both hands for most of cases). Figure 12 visually illustrates how well the predicted values fit the measured values. Figure 13 exhibits the normalized vectors of $(\mathbf{p}_1, \mathbf{p}_2)$ denoted $(\mathbf{p}_1^\star, \mathbf{p}_2^\star)$. As seen in this figure, for each hand, the two vectors are almost orthogonal to each other; and for both hands, they are nearly symmetric. The physical meaning of this reflection is that, in respect of a polar coordinate frame centered on the shoulder joint, the first synergy represented by $\mathbf{p}_1$ seems to generate the hand-force in the

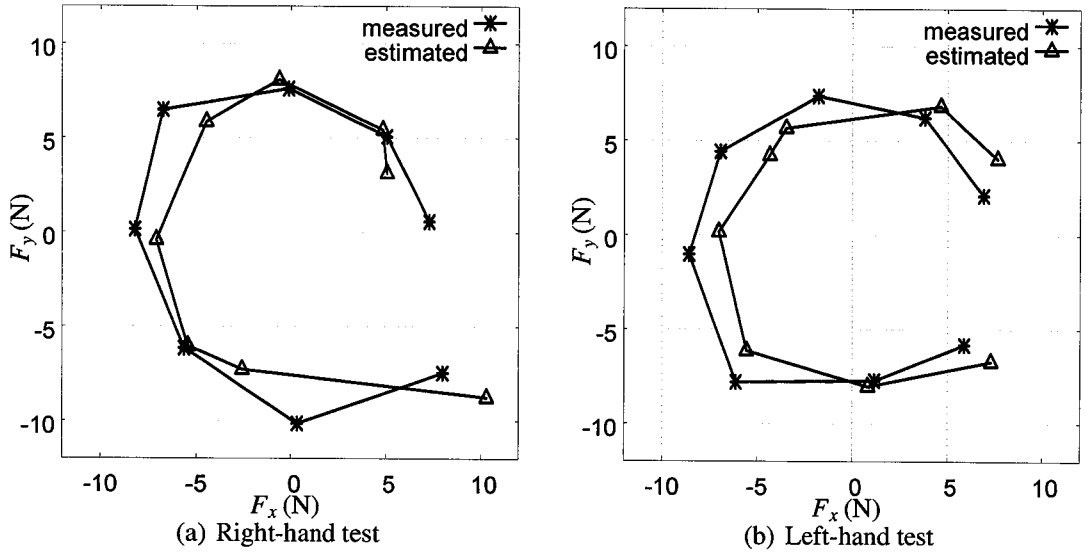

Figure 12: Hand-force and its estimation of right-hand test (left graph) and those of left-hand test (right graph).

angular direction and the second synergy represented by $\mathbf{p}_2$ seems to induce the hand-force in the radial direction. This result suggests that we can control movement by adjusting the hand-forces, which can be regulated by changing the weight of (w_1, w_2). Hence, it suggests a simple method to deal with the redundancy problem in the control of muscle-like robots. That is, using a few number of muscle synergies extracted from A-A ratios of EMG signals we can control pairs of antagonistic muscles and can consequently activate limb movements.

Along the same line, Ivanenko *et al.* [49] applied PCA to EMGs collected from 12-16 muscles in a walking movement. They found that five component factors accounted for about 90% of the total EMG patterns of activation muscles. However, they were unable to interpret how these factors functionally group the muscles and how they relate to force demand during locomotion. In this study we applied PCA to the A-A ratios derived from EMGs instead. This analysis has two advantages. One advantage is that the method offers a smaller dataset, which makes the analysis less tedious. The other advantage is that using PCA algorithm on the dataset of A-A ratios, which is related to the kinematics, the reduced

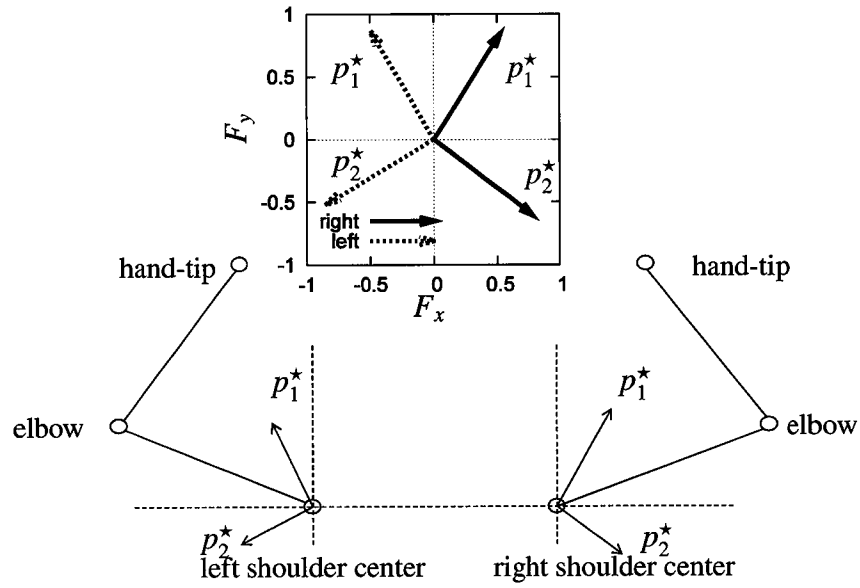

Figure 13: Synergy force vectors.

dataset would reveal the relationship between muscle activations and the hand-force production. Indeed, regression analysis results implied a strong relationship between the two identified synergies corresponding to the two PCs resulting from PCA and the hand-force produced. This method is also applicable to extract the muscle synergies of the human lower limb movements. Using the same measurement and analysis methods, we decomposed two patterns of the human running [43], walking [20], and pedaling [44]. Moreover, this method is also applicable to extract muscle synergies of multi-joint movements in 3-dimensional space [33]. We found three synergies that could represent for the muscle activities of 12 muscles of the human upper limb movements in 3-dimensional space.

3.4 A novel framework of human motor control

Based on the results of PCA and the regression analysis on EMGs discussed above, we hypothesize a novel framework for neural-mechanical control of the human arm. The general control scheme of the proposed framework is illustrated in Fig. 14(a). An example of using the framework to explain the hand-force production task is illustrated in Fig. 14(b). The motor control procedure includes the following steps:

1. The controller determines the task variables (the hand-forces **F**). The task variables may include feedback elements.

2. The hand-forces are converted into synergy variables reflecting muscle synergies represented with reference to a polar coordinate frame $((w_1, w_2))$.

3. Synergy variables are transformed into A-A ratio as

$$\delta \mathbf{r} = w_1 \mathbf{s}_1 + w_2 \mathbf{s}_2. \tag{38}$$

   which corresponds to (36).

4. Muscle commands are generated from A-A ratio and A-A activity. Following (25) muscle activities can be derived from

$$\begin{aligned} m_{2i-1} &= r_i a_i, \\ m_{2i} &= (1 - r_i) a_i \end{aligned} \tag{39}$$

   where i indicates the muscle pair index.

Though here we omitted the details of A-A activity, task variables include the endpoint (hand) stiffness, which is transformed into A-A activity, another variable to represent the activity of an antagonistic muscle pair.

This framework, based on the analysis results of EMG signals, is expected to be effective for the control scheme of musculoskeletal robots because of its simplification and flexibility. The only one important procedure in the synergy-based control scheme is to determine the desired synergy variables based on the desired task variables. This framework brings benefit to the redundancy problem since it uses a small number of variables to generate behavior movements. Moreover, it clarifies the function of synergies in producing forces, an important aspect of motor control. In a related study of cat locomotion, Drew *et al.* [42] suggested a model for motor cortex control. They identified synergies by a

novel associative cluster analysis based on the onset and offset of EMG activities, providing a flexible definition of synergies. However, they were unable to explain the underlying procedure of producing force.

3.5 Summary

This chapter presents the analysis of the human upper limb movement in an isometric task. We assessed the muscle synergies extracted from the A-A ratios of the measured EMGs. The analysis of muscle synergies based on A-A ratios is less tedious compared to that based on original EMGs. In addition, it helps to clarify the physical meanings of muscle synergies more clearly. Two synergies were identified, one relating to the angular movement and the other resulting in the radial movement, referring to a polar coordinate frame centered on the shoulder joint. This result suggests a possibility of generating behavioral movements by using only two synergies patterns. The framework, which was devised based on the outcomes of the human analysis, is simple and flexible to be applicable for robotic systems and for different tasks.

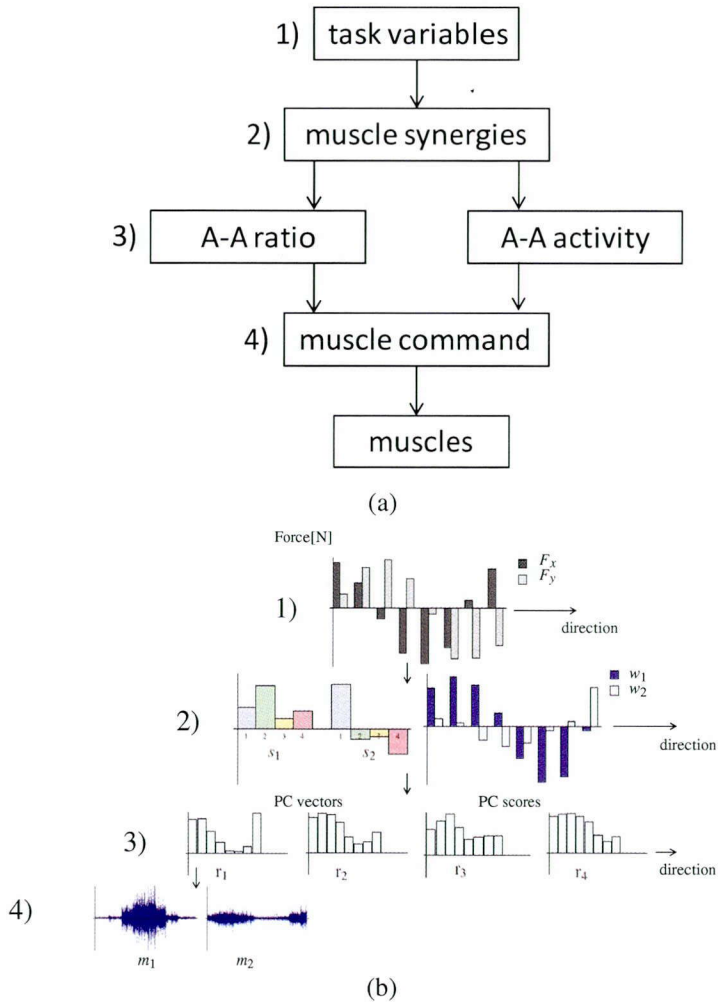

Figure 14: 14(a) Scheme of human motor control, 14(b): an example of hand-force generation scheme (right hand). The mechanism of the hand-force generation in 14(b) can be interpreted as follows. 1) The controller gets the task variables information (hand-forces (F_x, F_y)) and 2) identifies the synergy variables. 's1' and 's2' indicate PC1 and PC2 vectors, respectively. Each bar indicates the element corresponding to $\{r_1, r_2, r_3, r_4\}$, respectively. All of the elements of PC1 vector are positive, implying a similar contribution of all muscle extension. PC2 vector indicates a significant difference of $\{r_1, r_4\}$ compared to the others; thus, implying a simultaneous contribution of the shoulder extension ($r_1 > 0$) and elbow flexion ($r_4 < 0$). 3) From these PCs, A-A ratios at each movement are obtained. This expression implies the co-contraction among muscles within the antagonistic pairs. For example, the first bar of r_1 represents for the ratio of m_1 and m_2 towards ($F_x = 8N, F_y = 0N$). At this state, the high value of r_1 indicates that m_1 exceeds m_2, or the shoulder joint is extended. 4) Generates muscle commands to activate muscles, e.g., at the state of shoulder-joint extension the muscle activities $\{m_1, m_2\}$ are generated, activating these muscles to extend the shoulder joint, thus, producing a hand-force towards the desired force. This is valid for other force directions, and this process is valid for other muscle pairs' activation.

CHAPTER IV

IMPLEMENTATION OF MUSCLE SYNERGY IN MUSCULOSKELTAL ROBOT CONTROL

4.1 Introduction

Robots have been playing an important role in the human society. They involve in many fields of the human life, such as in manufacturing, entertainment, and especially in rehabilitation; and even replace human in several hazardous fields which are unsafe for humans to work in or in delicate work which require thorough accuracy that humans cannot perform. Robotics, therefore, are edged projects. Among various types of robots, the robots involving in cooperation tasks with human receive much more consideration. It is optimal to design the robots that can mimic the human motions. The more flexible and adjustable the robots become, the better they can contribute to the human tasks. In the previous chapter, we proposed a novel framework of motor control for the upper-limb movement, which is based on the synergy and equilibrium point controls. In this chapter, we present the implementation of the framework to pneumatic-driven robot systems. Verification experiments with a pneumatic-driven robotic arm will be included.

4.2 Synergy-based control method

The framework presented in the previous chapter was devised based on the results of human synergy analysis in an isometric task. However, we expect that this method can be extended to the movements in a larger scope, such as a reaching task. To verify the efficacy of the synergy control, we applied it to a pneumatic-driven robotic arm (the PAM model described in Section 2.1.3) with two joints and six pneumatic artificial muscles to perform a reaching task in a horizontal plane.

First, we modified the definitions of A-A ratio and A-A activity by considering the correspondence between muscle commands m_i and pressure commands p_i and the PAM model presented in Section 2.1.2, such that

$$R_i = \frac{p_{2i-1}}{p_{2i-1} + p_{2i}},$$
$$A_i = p_{2i-1} + p_{2i} \tag{40}$$

where $(i = 1, 2, 3)$ indicates the PAM pair index. Given A-A ratio R_i and A-A activity A_i, the pressure commands p_{2i-1} and p_{2i} can be derived as

$$p_{2i-1} = R_i A_i,$$
$$p_{2i} = (1 - R_i)A_i. \tag{41}$$

Second, we determined muscle synergies for the robotic arm since muscle synergies extracted from EMG signals ($(\mathbf{s}_1, \mathbf{s}_2)$ in (38)) are not directly applicable to the robotic arm whose musculoskeletal structure is different from that of a human. In the following, we explain how to determine muscle synergies for the robotic arm.

In the hand-force production task, we regarded the hand-forces represented with reference to a polar coordinate frame as the synergy variables. Here, we regard hand-tip displacements defined with reference to the same polar coordinate frame as the synergy variables and assume the relationship between synergy variables and A-A ratio

$$\mathbf{w} = \mathbf{H}\delta\mathbf{r}, \tag{42}$$

where $\mathbf{w} = \begin{bmatrix} w_1, w_2 \end{bmatrix}^T$ are the synergy variables and $\mathbf{H}$ is the Jacobian matrix representing the infinitesimal relationship between the synergy variables and a deviation of A-A ratios. If we experimentally obtain $\mathbf{H}$, muscle synergies for the robotic arm $(\mathbf{s}_1, \mathbf{s}_2)$ can be determined by using the pseudo-inverse of $\mathbf{H}$. That is,

$$\mathbf{H}^+ = \begin{bmatrix} \mathbf{s}_1 \ \mathbf{s}_2 \end{bmatrix}. \tag{43}$$

The steps to determine $\mathbf{H}$ include:

1. Run the robot with a set of random A-A ratios, $\mathbf{R} = \{\mathbf{R}_1, \mathbf{R}_2, \dots\}$ where $\mathbf{R}_i$ is a 3-dimensional vector of A-A ratio at the i-th trial, and collect synergy variables $\mathbf{V} = \{\mathbf{w}_1, \mathbf{w}_2, \dots\}$.

2. Calculate the Jacobian matrix $\mathbf{H}$ from the linear regression model of (42), giving

$$\mathbf{H} = \mathbf{V}\Delta\mathbf{R}^T(\Delta\mathbf{R}\Delta\mathbf{R}^T)^{-1}. \tag{44}$$

4.3 Experimental setup

4.3.1 The task

We implemented the synergy control method in a robotic arm to perform a reaching task. The task was to move the robot's hand-tip from an initial position towards a target position with a displacement $\delta\mathbf{x}_\mathrm{d} = \left[\delta x_\mathrm{d}, \delta y_\mathrm{d}\right]^T$. The hand-tip movement was tracked and recorded.

4.3.2 Apparatus

The robotic arm was built with six PAMs (McKibben, Kanda Tsushin Kogyo). The robot's mechanical structure is illustrated in Fig. 3 and the robotic arm's appearance is displayed in Fig. 4. The robot's PAMs corresponded to three antagonistic muscle pairs of human (see Table I); thus the A-A ratios of the robot $\{R_1, R_2, R_3\}$ corresponded to those of human $\{r_1, r_2, r_3\}$.

A computer computed commands according to the targets input from the keyboard and transferred them through A/D converters (PCI-3346A, PCI-3522A) to a pneumatic regulator (APC-C300-16, Hitachi Medical Corp.). The regulator converted voltage commands into pressure commands and then sent those to an air compressor (JUNAIR12-25). The air compressor supplied air pressures to each pneumatic artificial muscle, making the robotic arm to move accordingly. Motion tracking devices (OptiTrack system) captured the hand-tip movement. The experimental system is illustrated in Fig. 15.

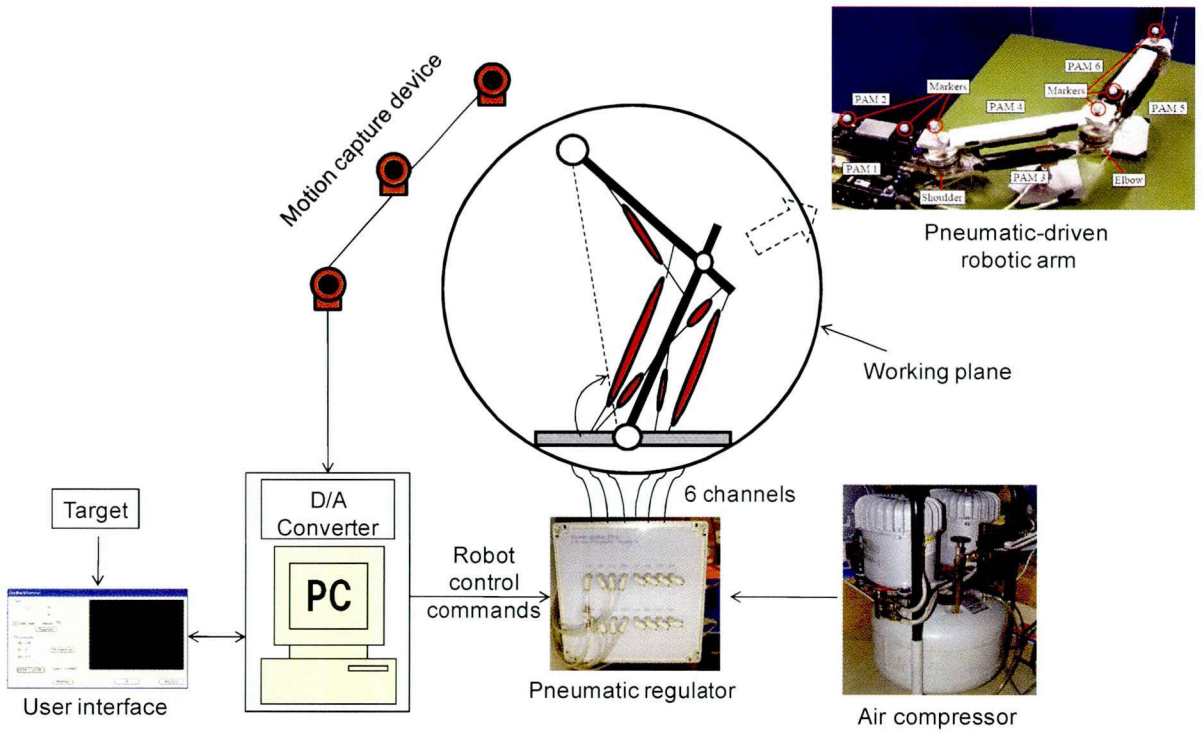

Figure 15: Robotic arm system.

4.3.3 Muscle synergies for the robotic arm

We experimentally obtained the Jacobian matrix $\mathbf{H}$ in (42) by following the steps described in Section 4.2. Using the pseudo-inverse of $\mathbf{H}$, we can describe the inverse relation of (42) as

$$\delta\mathbf{r} = w_1\mathbf{s}_1 + w_2\mathbf{s}_2 \tag{45}$$

which corresponds to (38).

Considering the relationship $\delta\boldsymbol{\theta} = \mathbf{A}\delta\mathbf{r}$ in (24) and $\delta\mathbf{x} = \mathbf{J}\delta\boldsymbol{\theta}$ (where $\mathbf{J}$ is the Jacobian matrix representing the relationship between the joint displacement and the hand-tip displacement $\delta\mathbf{x} = \left[\delta x, \delta y\right]^T$), (45) is converted into

$$\begin{aligned}\delta\mathbf{x} &= w_1\mathbf{JAs}_1 + w_2\mathbf{JAs}_2 \\ &= w_1\mathbf{p}_1 + w_2\mathbf{p}_2\end{aligned} \tag{46}$$

where $\mathbf{p}_1 = \mathbf{JAs}_1$ and $\mathbf{p}_2 = \mathbf{JAs}_2$ are muscle synergies (called synergy displacement vectors) represented in terms of the hand-tip displacement. Figure 16 illustrates the normalized synergy displacement vectors $(\mathbf{p}_1^\star, \mathbf{p}_2^\star)$ estimated by using the regression model of (46). The regression model to estimate the deviation of the hand-tip position from synergy variables (w_1, w_2) is:

$$\delta\mathbf{x} = \begin{bmatrix} 88.18 \\ 128.0 \end{bmatrix} \mathbf{w}_1 + \begin{bmatrix} 174.8 \\ -137.0 \end{bmatrix} \mathbf{w}_2 \tag{47}$$

with regression coefficients $R^2 = 0.97$ for δx and $R^2 = 0.98$ for δy. These vectors $(\mathbf{p}_1^\star, \mathbf{p}_2^\star)$ are similar to the synergy force vectors in the hand-force production task of the human case (see Fig. 13). As shown in Fig. 16, the first synergy seems to generate the angular-directional movement while the second synergy seems to induce the radial-directional movement, with reference to a polar coordinate frame centered on the shoulder joint. This result suggests the validity of the model (46) and confirms the physical meaning of the muscle synergies in generating movement.

4.4 *Performance of the synergy control*

4.4.1 Feedforward synergy control

Let us consider the reaching task, which is to move the robot's hand-tip from an initial position towards a target position with a displacement $\delta\mathbf{x}_\mathrm{d} = \left[\delta x_\mathrm{d}, \delta y_\mathrm{d}\right]^T$. $\delta\mathbf{x}_\mathrm{d}$ are the task variables in this task. The only one important procedure in the synergy-based control scheme (presented in Section 3.4) is to determine the desired synergy variables $\mathbf{w}_\mathrm{FF} = (w_{1\mathrm{d}}, w_{2\mathrm{d}})$ corresponding to the desired task variables $\delta\mathbf{x}_\mathrm{d}$. In feedforward (FF) synergy control, the desired synergy variables $\mathbf{w}_\mathrm{FF}$ are calculated by the model (47) with a displacement of $\delta\mathbf{x}_\mathrm{d}$. The synergy variables $\mathbf{w}_\mathrm{FF}$ are then transformed into A-A ratio, from which pressure commands of pneumatic artificial muscles are generated. Figure 17(a) illustrates a trial with a small target displacement in x direction ($\delta\mathbf{x}_\mathrm{d} = \left[40, 0\right]^T$ mm). A quick response of FF synergy control was observed but a steady-state error was involved, which was due to the model uncertainties. Note that A-A activity was fixed in this task to

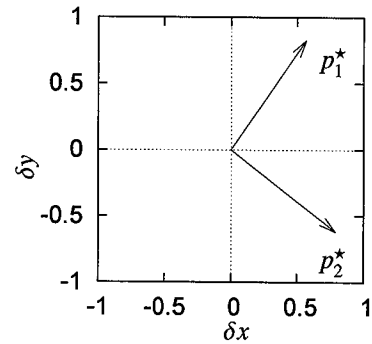

Figure 16: Synergy vectors estimated from PC scores using regression analysis in FF synergy control mode. The first synergy vector seemed to generate angular-directional movement while the second synergy vector seemed to induce the radial-directional movement, regarding a polar coordinate system centered on the shoulder joint. This functional synergy vectors are similar to the synergy force vectors in the hand-force production task of the human case.

show the efficacy of the proposed control scheme clearly.

4.4.2 Feedback synergy control

It is well-known that the use of feedback (FB) loops makes the system response relatively insensitive to the model uncertainties. For example, a conventional PID-type FB control can be implemented to the synergy control. The feedback signals $\mathbf{e} = \delta\mathbf{x} - \delta\mathbf{x}_\mathrm{d}$, the error between the desired task variables and the measured ones, are converted into the synergy variables $\mathbf{w}_e$ through the model (47) with $\mathbf{e}$ instead of $\delta\mathbf{x}_\mathrm{d}$ as in FF synergy control. Furthermore, the synergy variables are modified and updated with PID control algorithm as

$$\mathbf{w}_\mathrm{FB} = K_p\mathbf{w}_e + K_i\int \mathbf{w}_e dt + K_d\dot{\mathbf{w}}_e \tag{48}$$

where (K_p, K_i, K_d) are gains of the PID controller. The synergy variables $\mathbf{w}_\mathrm{FB}$ are then transformed into A-A ratio related to pressure commands. Since the correction of the FB starts only after it receives the feedback signals (the error), a very large error may cause an unacceptable upset in a process before the controller can compensate for it. This cause the system overshot. Choosing appropriate feedback gains can help to tune the system

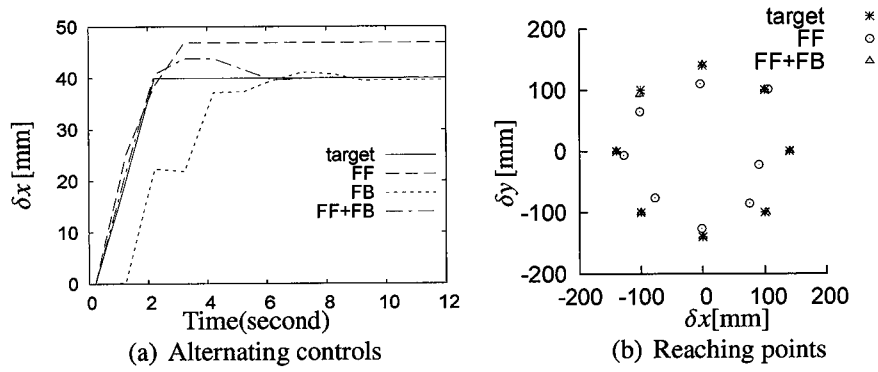

Figure 17: Robot performance. 17(a) shows the robot performance in different control modes (single FF synergy control, single FB synergy control, and combination FF+FB synergy control modes). FF synergy control mode is faster than FB synergy control mode, but less accurate. FF+FB synergy control mode is more accurate than FF synergy control mode and is faster than FB synergy control mode. 17(b) illustrates the reaching points in three control modes with a larger target displacement, indicating the accuracy of FF+FB synegy control mode compared to the FF synergy control mode.

smoothly. However, how to choose feedback gains to obtain smooth response is difficult. One alternating solution is to compensate small errors instead of a big error at once. The task variables, therefore, need to be adjusted by small portions to keep the performance smooth and to avoid making the system overshot. Figure 17(a) illustrates a trial using the FB synergy control with the same small target displacement as that was tested with the FF synergy control above. As seen in this figure, the FB synergy control is effective in terms of accuracy but not in terms of execution time.

4.4.3 Feedforward and feedback synergy control

Although FF synergy control could manipulate the robotic arm to reach a position close to the target, there was a deviation existing. On the other hand, the result of FB synergy control indicated its effectiveness in terms of accuracy. Hence, we designed a control scheme combining FF and FB synergy controls. FF synergy control was to drive the robot towards the target and FB synergy control was to reduce the error between the reaching point and the target point. In this FF + FB synergy control, the synergy variables

were modified as

$$\mathbf{w}_{\mathrm{FF+FB}} = \mathbf{w}_{\mathrm{FF}} + \mathbf{w}_{\mathrm{FB}}. \tag{49}$$

As seen in Fig. 17(a)), when using FF+FB synergy control, the robot can perform a smooth movement with much shorter execution time compared to when using FB synergy solely. Figure 17(b) illustrates the robot reaching performance with a larger target displacement. When using FF + FB synergy control, the robot's performance was much more accurate compared to that when merely using FF synergy control.

4.4.4 Learning control

For robot manipulators that perform repetitive tasks, learning control is a perspective control method. The first English paper about the learning control was published in 1984 [39]. Since then, the learning control has been vigorously studied.

Let $\mathbf{u}_i(t)$ and $\mathbf{x}_i(t)$ be the input and output of the i-th control process of a dynamic system, $\mathbf{u}_{i+1}(t)$ be the input for the $(i+1)$-th control process, and $\mathbf{e}_i(t) = \delta\dot{\mathbf{x}}_i(t) - \delta\dot{\mathbf{x}}_{\mathrm{d}}(t)$ be the error in the i-th process. A typical learning control process can be written as follows.

$$\mathbf{u}_{i+1}(t) = \mathbf{u}_i(t) + \Gamma(t)\,\dot{\mathbf{e}}_i(t) + \Psi(t)\mathbf{e}_i(t) \tag{50}$$

where $\Gamma(t)$ and $\Psi(t)$ are coefficient matrices. The convergent condition is

$$\|\dot{\mathbf{e}}_i(t)\| \to 0 \quad \text{as } i \to \infty. \tag{51}$$

For simplicity, in (50), the coefficients are set to be constant gains K_d and K_i. The control law becomes

$$\mathbf{u}_{i+1}(t) = \mathbf{u}_i(t) + K_d\dot{\mathbf{e}}_i(t) + K_i\mathbf{e}_i(t). \tag{52}$$

To achieve more precise control, the time lead in the control process is addressed as

$$\mathbf{u}_{i+1}(t) = \mathbf{u}_i(t) + K_d\dot{\mathbf{e}}_i(t-\tau) + K_i\mathbf{e}_i(t-\tau) \tag{53}$$

where τ is the time lead, $\{K_d, K_i\}$ are gains.

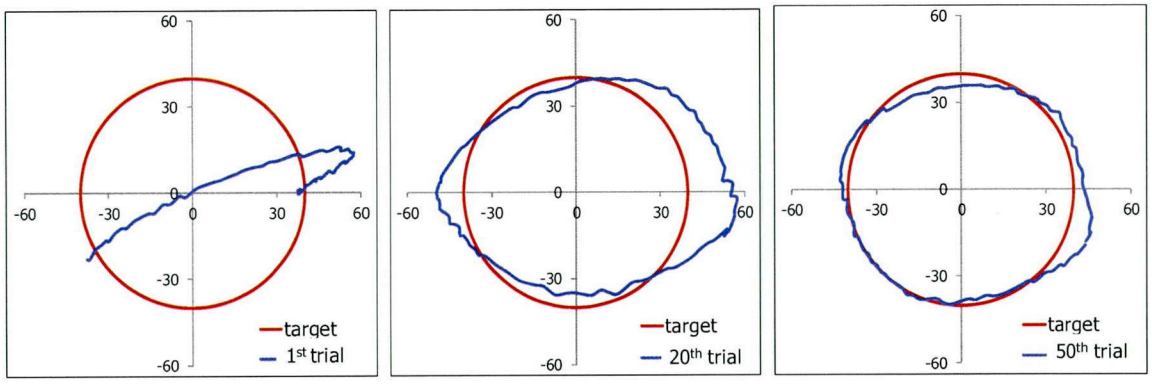

(a) (b) (c)

Figure 18: Learning control with crank-rotation task.

The learning task that we wanted the robotic arm to perform was a crank-rotation task. That was to move the hand-tip in the counterclockwise rotation, drawing a circle with a given radius. One cycle was expected to be completed in one second.

The task variables in this case are the desired running target $\delta\mathbf{x}_\mathrm{d} = \left[\delta x_\mathrm{d}, \delta y_\mathrm{d}\right]^T$. The synergy variables $\mathbf{w}_\mathrm{FF}$ now are modified as

$$\mathbf{w}_i(t) = \mathbf{w}_{i-1}(t) + K_d\dot{\mathbf{e}}_{i-1}(t-\tau) + K_i\mathbf{e}_{i-1}(t-\tau). \tag{54}$$

The synergy variables are then converted into pressure commands supplied to the pneumatic artificial muscles. When the error $\mathbf{e}_i(t)$ is acceptable, the iteration can be stopped.

Figure 18 presents a crank-rotation learning process of the robotic arm, drawing a circle of 40 mm in radius. Each circle was completed in one second. The horizontal and vertical axes indicate the robot hand-tip's displacement in x- and y-directions [mm], respectively. As shown in these graphs, the trajectory is gradually improved. The trajectory of the 20-th trial is almost a close circle and it is less distorted than the trajectory of the first trial (see Fig. 18(b) and 18(a)). The robot's trajectory then gradually gets closer to the target trajectory. From about the 50-th trial, the robot's trajectory is close to the target trajectory as illustrated in Fig. 18(c).

4.5 Summary

Applying the proposed synergy control method to a pneumatic-driven robotic arm, we validated the efficacy of the novel hypothesis of motor control for the upper limb movement. Although A-A activity was fixed in this task to show the efficacy of the proposed control scheme clearly, we have investigated human adaptation to variable-stiffness assistance from the view point of muscle synergy analysis based on A-A activity and reported that stiffness control of the knee exoskeleton implementing the A-A activity of an able-bodied person reduced all muscle activities of the user's lower limbs [7]. In addition, utilizing the synergy control method, our group has succeeded in controlling a pair of pneumatic-driven robotic legs in performing pedaling movements [44]. Although the pedaling project also implemented the synergy control method based on A-A ratios since it specially focused on the equilibrium posture, one important phase of movement besides the stiffness control, it suggested the important of A-A activity in movement control to achieve smoother and more human-like pedaling movement.

CHAPTER V

ROLE SHARING IN A COORDINATED TASK

5.1 Introduction

The use of robots in cooperative interaction tasks with humans is increasing. An understanding of the cooperation between two human subjects in a coordinated movement would benefit to the performance of robots which involve in coordinated tasks with human. In a coordinated task, there are multiple ways to combine the redundant controls [13]. From empirical understandings of the facts that an appropriate division of roles often improves work performances [21, 22, 23], and muscle activities have an effect on movement [27], this experiment focuses on the role division of two persons in a crank-rotation task by examining the muscle activities and the hand-forces of the two members.

Reed's [24] defined two kinds of cooperative strategies when two persons works together. One strategy is 'active/inert' dyad. That is, one member provides a force toward the target in early of the trial and then late in the trial that subject provides force to decelerate the motion. The other member creates counterproductive force all the time. The other strategy is 'specialized' dyad. That is, one member mainly contributes to the acceleration phase while the other member mainly contributes during the deceleration phase. He observed that the dyads worked faster than their constituent members working alone. However, he did not offer a clear explanation for the improvement of the task performance when two members working together.

In this experiment, we approached the role sharing between two human subjects in a coordinated task from the viewpoints of muscle activity patterns and hand-force patterns. We expected to find correlation patterns of the dyad members in the dyad performance in order to improve the synergy-based control for musculoskeletal robots so that they can work

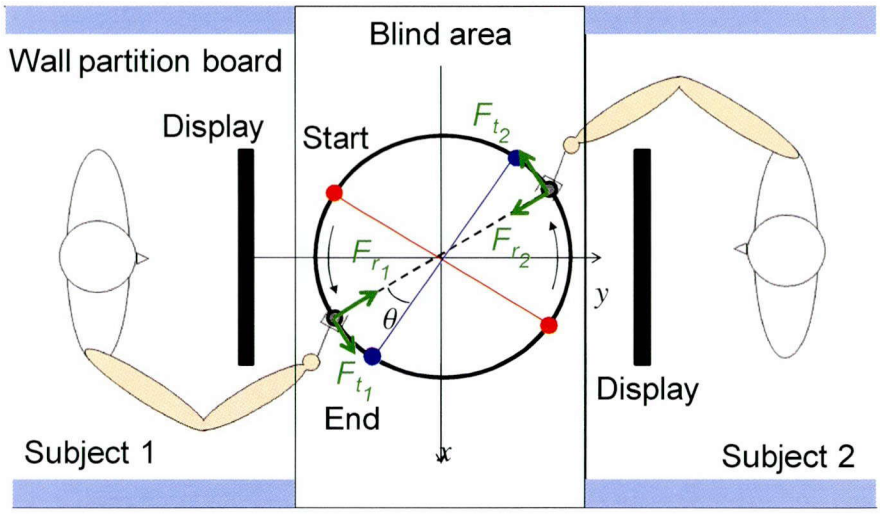

Figure 19: Experimental setup, top view.

more gently compliantly with humans. This chapter presents the details of the experiment and experimental results with discussions.

5.2 *Materials and method*

5.2.1 The task

Subjects were asked to move a crank into a target area as quickly as possible and to hold it there until a new target appeared. Each experimental run had 40 trials, including clockwise rotations and counterclockwise rotations. Resting time between each rotation was within 1-3 seconds, and was set randomly.

5.2.2 Subjects

Two healthy volunteers (male, right-handed), aged 21 and 24, participated in the experiment. All of them gave informed consent conforming to the Ethics Committee of Osaka University. Call the subjects O and S.

5.2.3 Experimental setup

Figure 19 illustrates the experimental setup. F_t stands for tangential force. F_r stands for radial force. The crank with two handles is hidden behind a black curtain so that two

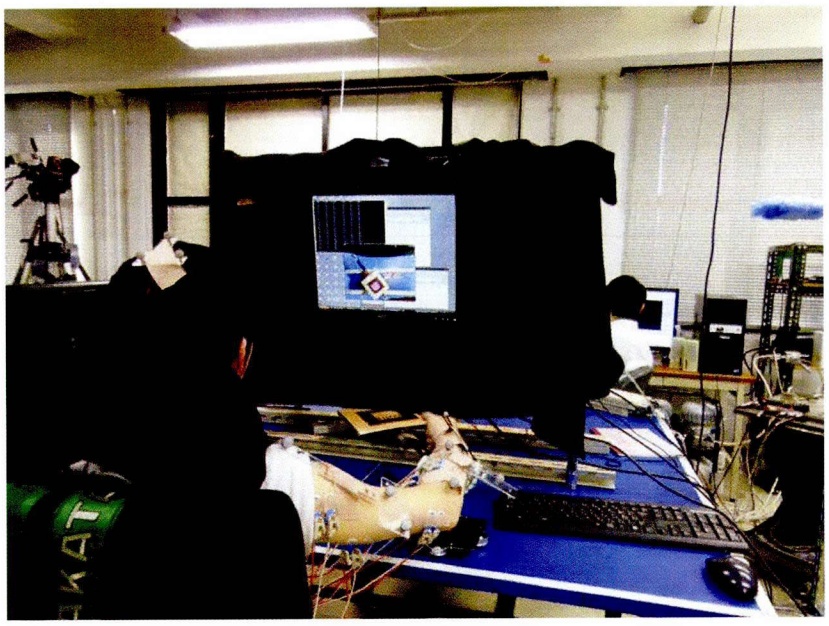

(a) Single trial

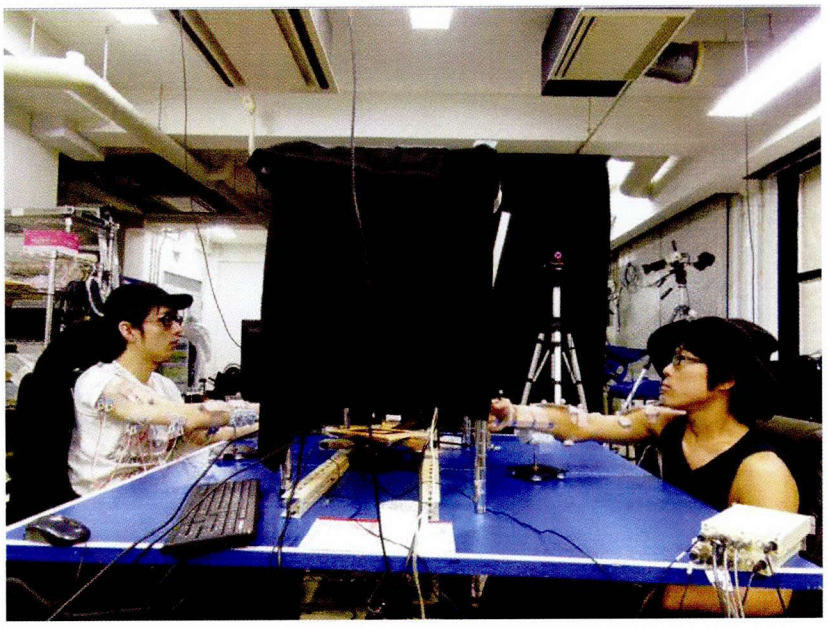

(b) Dyad trial

Figure 20: Experimental view.

subjects cannot see each other during the test. A force sensor (USL06-H5-200, TecGihan) is attached under each handle to measure the hand-force at 100 Hz. The arm movement of each subject is tracked by the motion capture system (Optitrack; NaturalPoint, Inc.) at 100 Hz. A separate camera is used to capture the crank movement. The crank movement, together with targets, is shown on the displays hang in front of each subject. The crank angle θ is the angle between the crank and the x-axis. The targets (end points), identical for two subjects, are set to be within $\theta = 50 - 60$ deg on the right side to $\theta = 140 - 150$ deg on the left side. The monitors also display the elapsed time and the trial information. Muscle activities are observed through EMGs. EMGs are recorded by using a multi-telemeter system (WEB-5000, Nihon Kohden) for one subject and by another multi-telemeter system (WEB-7000, Nihon Kohden) for the other one, at 1000 Hz. All measurement devices are synchronized. The procedure to measure EMGs was similar to the EMGs measuring process described in Section 3.2.3.

Figure 20(a) illustrates a real experimental setup. The subjects sit comfortably on chairs, leaning on the chair's back. The subjects' shoulder joint, elbow joint, and wrist joint are in a horizontal plane. To reduce the gravitational effect, carts that can move freely in the work place are used to support the subjects' elbow. For analysis simplicity, subjects' wrist is fixed to prevent wrist movement. For the single task, only one subject performed the task. For the dyad task, two subjects performed the task together (see Fig. 20(b)).

First, each subject individually completed ten single trials (single O and single S). Next, we asked the subjects to perform the dyad task (dyad OS). Two subjects worked together to complete ten runs.

Measured EMGs of each trial were pre-processed. The pre-processed EMG signals and the measured hand-forces of each trial were averaged with respect to time. For details, please see Section 3.2.4.

Table 7: Execution time of dyads and single subjects

Execution time [second]	dyad OS	single O	single S
counterclockwise rotation	0.52	0.68	0.93
clockwise rotation	0.64	0.71	0.99

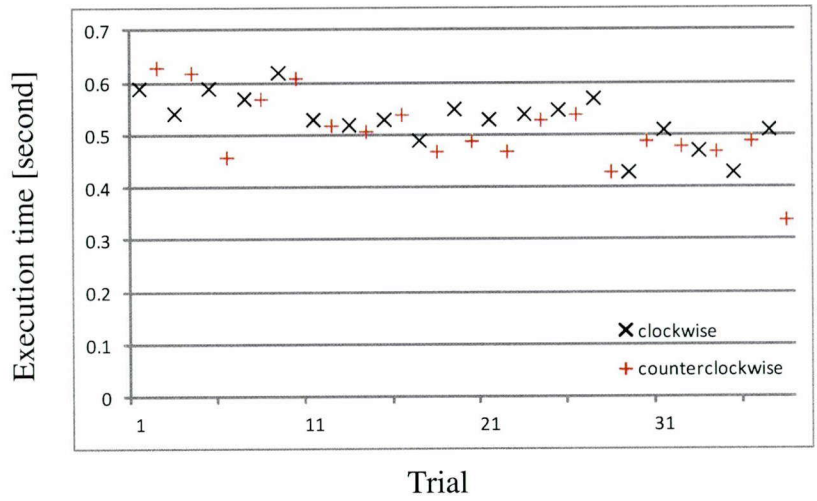

Figure 21: Improvement through trials during an experimental run (dyad trial).

5.3 *Improvement of performance in dyad work*

Execution time is the time for moving the crank from the start point to reach the end point. We confirmed that dyad performance achieved less execution time than single performance [24, 37]. Table 7 presents the averaged execution time of dyad OS, single O, and single S. As seen in this table, dyads completed the task faster than individuals. Moreover, the performance was improved through trials. The execution time gradually reduced from the beginning of the test until the end of the test (see Fig. 21).

5.4 *PCA results*

5.4.1 A-A ratio

For both single task and dyad task, the first two PCs contributed over 90% to the percentage variation of the A-A ratios of each subject (see Table 9). Therefore, it is reasonable to represent A-A ratios by using the first two PCs.

Table 8: Percentage of variation accounted for by the first two PCs (A-A ratio)

		Counterclockwise			Clockwise		
		PC1	PC2	Total	PC1	PC2	Total
Single trial	O	84.08	12.27	96.35	93.56	3.48	97.04
	S	73.68	21.69	95.37	70.80	23.59	94.39
Dyad trial	O	77.05	21.22	98.27	70.99	27.14	98.13
	S	52.93	45.07	98.00	61.42	33.55	94.97

5.4.1.1 PC scores

1. PC1 scores

   In the counterclockwise rotation

   - Dyad trials: PC1 scores of each dyad member were similar in shape (bang-bang type) but phase lag. Figure 22 illustrates the PC1 scores patterns of A-A ratio (rPC1) of dyad OS in nine trials in the counterclockwise rotation. As seen in this figure, rPC1 scores of subject O is phase lead in the first half of the trial but rPC1 scores of subject S is phase lead in the late half of the trial. This pattern is the specialized pattern. The phase lead increases through trial times. In the early trials (trial 1, 2, and 3), rPC1s of two members almost start at the same time, and have similar movements (see Fig. 22(a), 22(b), and 22(c)). From trial 4, the role division occurs more clearly as the phase lead between rPC1 of subject O and that of subject S more increases.

   - Single trials: in most cases, the PC1 score patterns of each subject were similar to the patterns of that subject in the dyad trials. Figure 23 shows the PC1 scores patterns of subject S and subject O in the single task. Subject S's pattern shows an acceleration in the first half of the trial but a weak adjustment in the late half of the trial. This pattern is different from the pattern of subject S in the dyad trials. In the dyad trials, his pattern implies a clear adjustment in the late half of the trial, following the lead of his partner O. Subject O's pattern in the single trials is similar to his pattern in the dyad trials, accelerating in the first half of

the trial and decelerating in the late half of the trial.

In the clockwise rotation:

- Dyad trials: rPC1 scores of each dyad member were similar and less phase lag. Figure 25 shows the rPC1 scores of dyad trials in the clockwise rotation. As seen in this figure, rPC1 scores of one subject are phase lead while rPC1 scores of the other subject move along (active/inert dyad).
- Single trials: The rPC1 score pattern of each subject in the single trials was similar to the rPC1 score pattern of that subject in the dyad trials.

2. PC2 scores

In the counterclockwise rotation:

- Dyad trials: PC2 scores of each dyad member were also similar in shape. Figure 26 demonstrates the PC2 scores (rPC2) of dyad OS in the counterclockwise rotation. As seen in this figure, rPC2 of two members have a similar startup, but in late of the trial, rPC2 of subject O raises up while rPC2 of subject S gradually reduces, indicating an adjustment of subject O to the movement and the passive movement of subject S (see Fig. 26(a), 26(b), 26(c), 26(d), and 26(e)). However, after five trials, the two members present more similar strategy. Their rPC2 have a similar startup and slowing down patterns, but different in phase. Subject O mostly leads the movement. This pattern is active/inert pattern.
- Single trials: the rPC2 score pattern of subject S keeps unchanged (see Fig. 27). Subject O's pattern shows an adjustment in the end of the trial, just similar to his performance in the dyad trials.

In the clockwise rotation:

- Dyad trials: the rPC2 scores of two dyad members were similar, but different in phase. Most of the cases, one member led the movement in the first half of the

trial and the other member led the movement in the late half of the trial, or this pattern is specialized pattern (see Fig. 28).

- Single trials: rPC2 pattern of each subject was similar to the pattern in the dyad trials but less adjustment in the end of the trial (see Fig. 29).

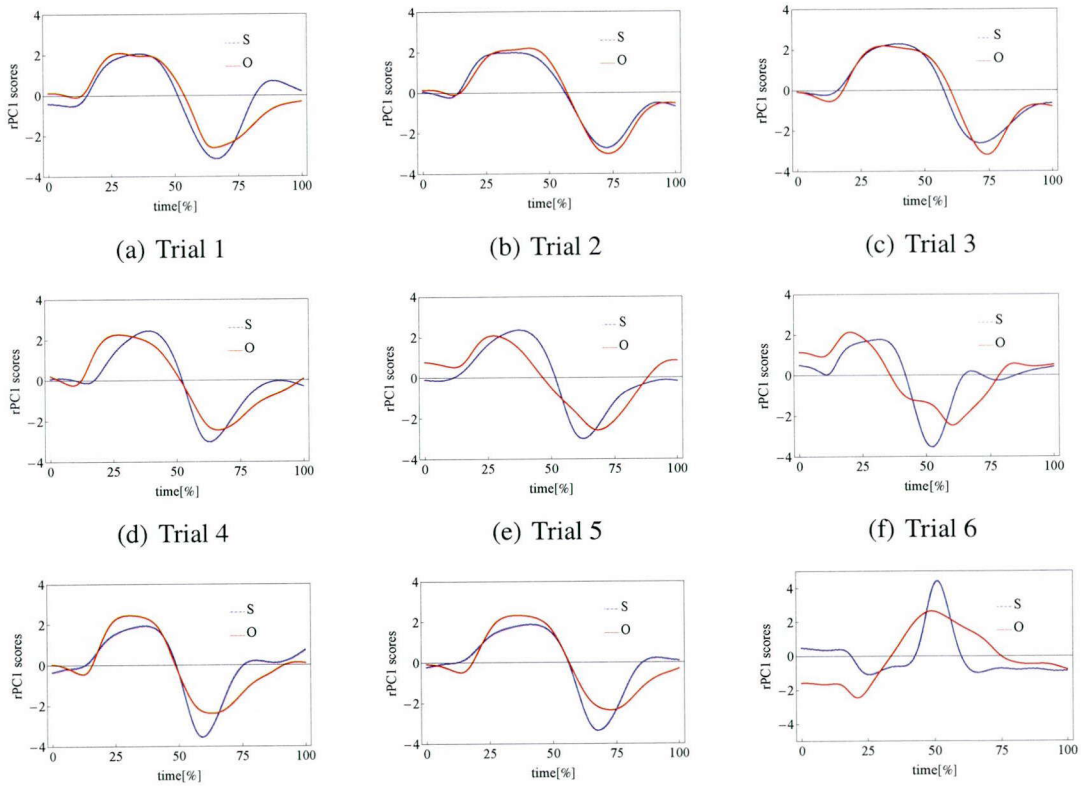

(a) Trial 1 (b) Trial 2 (c) Trial 3

(d) Trial 4 (e) Trial 5 (f) Trial 6

(g) Trial 7 (h) Trial 8 (i) Trial 9

Figure 22: PC1 scores of A-A ratio of dyad trials in the counterclockwise rotation.

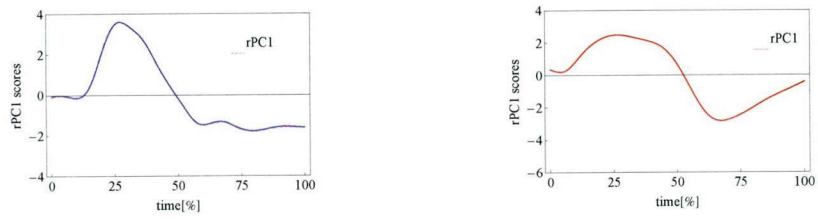

(a) Single S (b) Single O

Figure 23: PC1 scores of A-A ratio of individuals in the counterclockwise rotation.

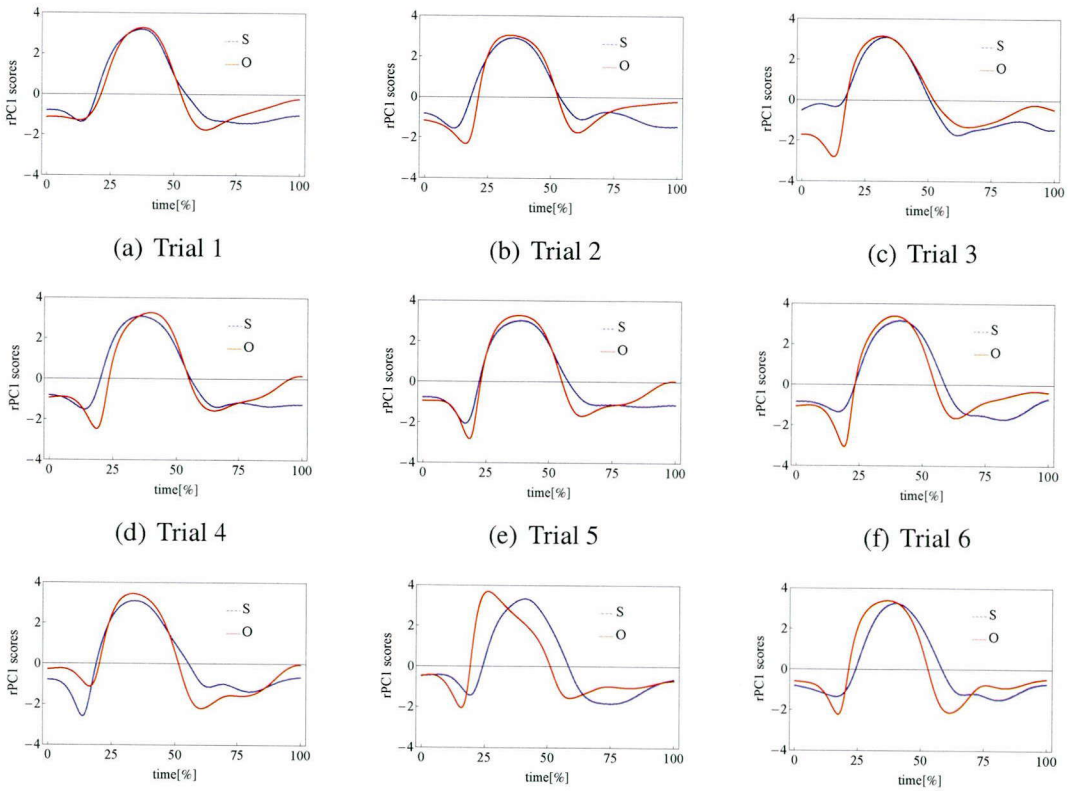

(a) Trial 1 (b) Trial 2 (c) Trial 3

(d) Trial 4 (e) Trial 5 (f) Trial 6

(g) Trial 7 (h) Trial 8 (i) Trial 9

Figure 24: PC1 scores of A-A ratio of dyad trials in the clockwise rotation.

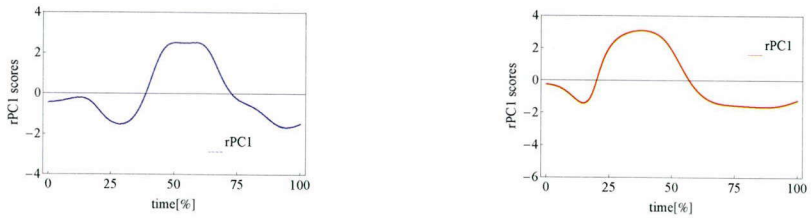

(a) Single S (b) Single O

Figure 25: PC1 scores of A-A ratio of individuals in the clockwise rotation.

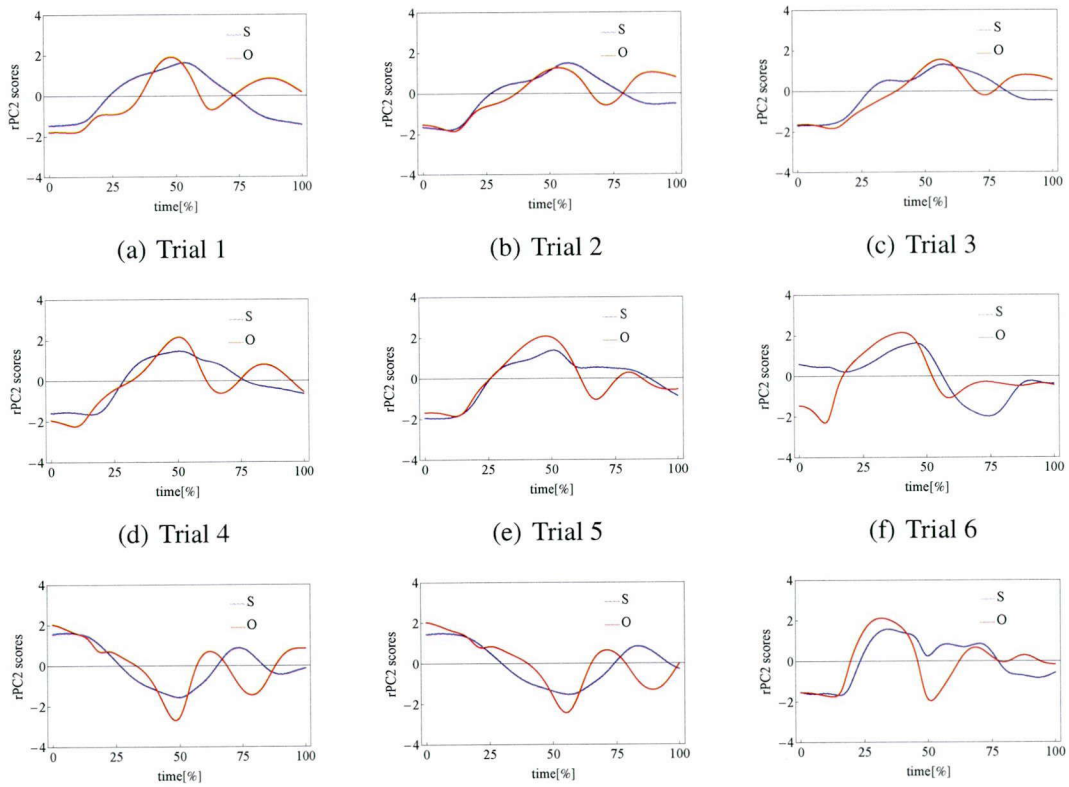

(a) Trial 1 (b) Trial 2 (c) Trial 3

(d) Trial 4 (e) Trial 5 (f) Trial 6

(g) Trial 7 (h) Trial 8 (i) Trial 9

Figure 26: PC2 scores of A-A ratio of dyad trials in the counterclockwise rotation.

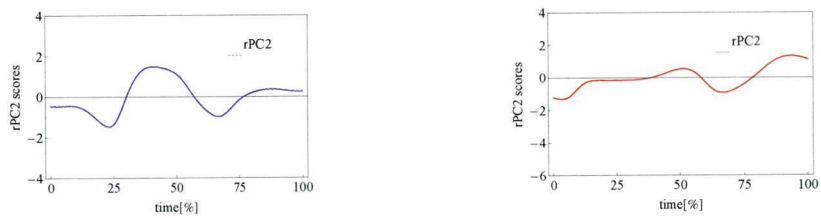

(a) Single S (b) Single O

Figure 27: PC2 scores of A-A ratio of individuals in the counterclockwise rotation.

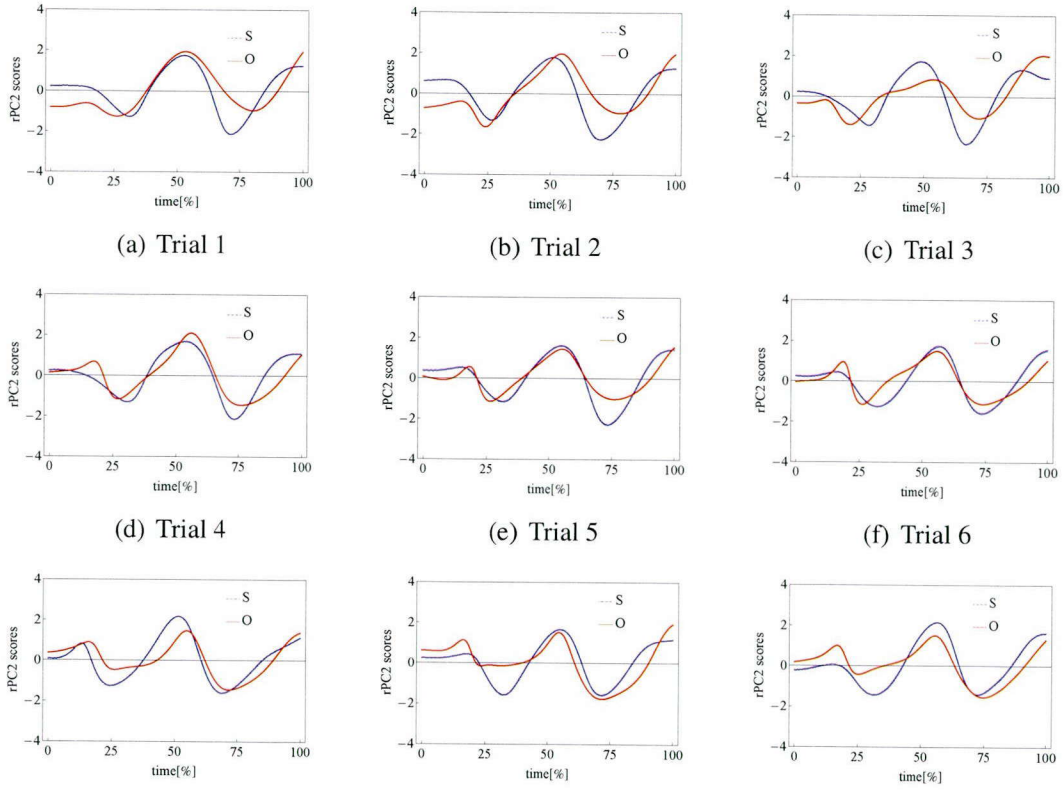

(a) Trial 1 (b) Trial 2 (c) Trial 3

(d) Trial 4 (e) Trial 5 (f) Trial 6

(g) Trial 7 (h) Trial 8 (i) Trial 9

Figure 28: PC2 scores of A-A ratio of dyad trials in the clockwise rotation.

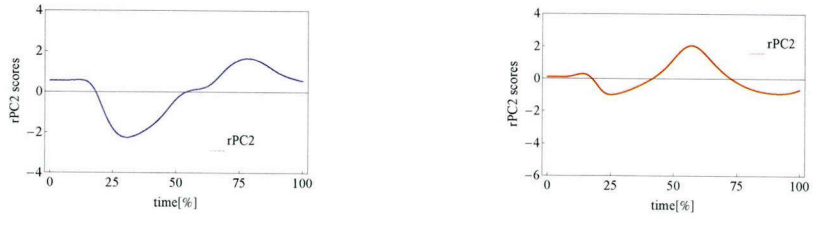

(a) Single S (b) Single O

Figure 29: PC2 scores of A-A ratio of individuals in the clockwise rotation.

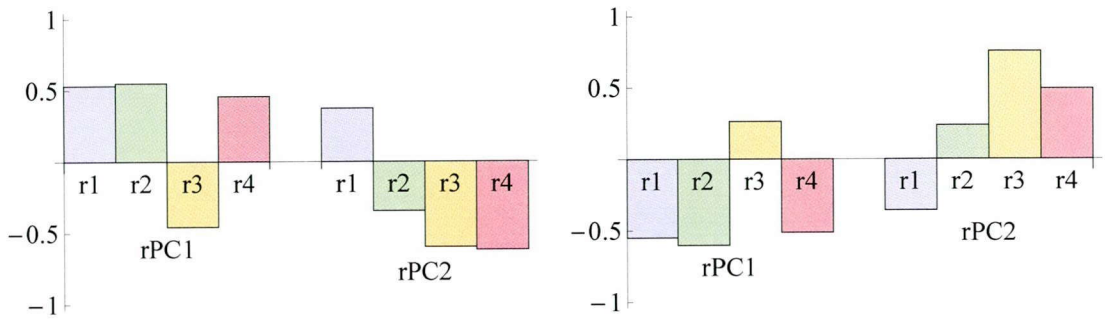

(a) Subject S (b) Subject O

Figure 30: PC vectors of A-A ratio of dyad trials in the counterclockwise rotation.

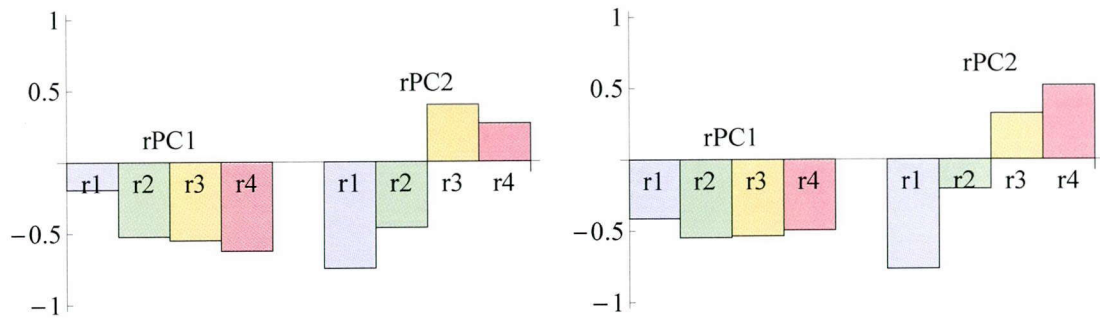

(a) Single S (b) Single O

Figure 31: PC vectors of A-A ratio of individuals in the counterclockwise rotation.

5.4.1.2 PC vectors

1. PC1 vectors

   In the counterclockwise rotation:

   - Dyad trials: PC1 vector of A-A ratio of each dyad member was similar. Figure 30 illustrates PC vectors of dyad OS in the counterclockwise rotation. For PC1 vectors (rPC1), the elements corresponding to $\{r_1, r_2, r_4\}$ are the same sign, which are different from the element corresponding to r_3. This pattern implies that the antagonistic muscle pair r_3 (the one-joint muscles pair around the elbow joint) works differently with the other pairs, extending/flexing while the other pairs flexing/extending, to produce the movement in the angular direction. The value of each element is approximately equal, indicating that the extending/flexing of each muscle pair is approximately equal.

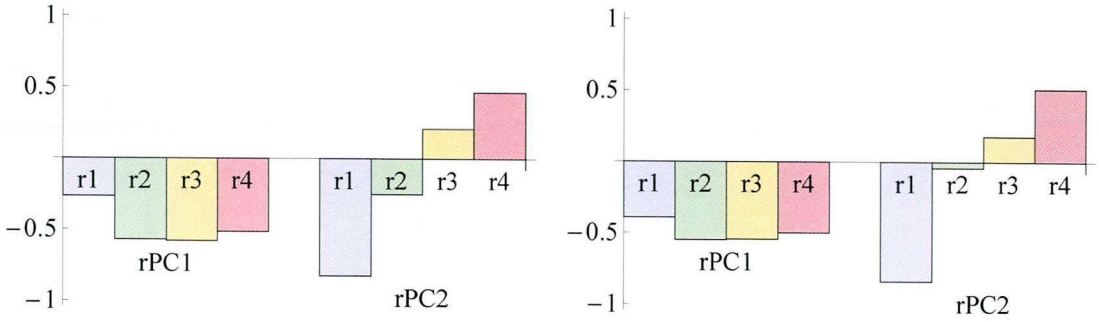

(a) Subject S (b) Subject O

Figure 32: PC vectors of A-A ratio of dyad trials in the clockwise rotation.

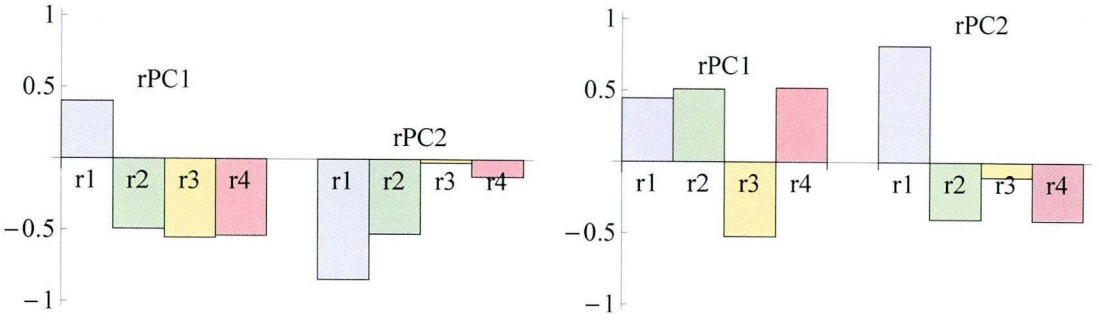

(a) Single S (b) Single O

Figure 33: PC vectors of A-A ratio of individuals in the clockwise rotation.

- Single trials: PC1 vectors of individuals are similar (see Fig. 31). All elements of rPC1 are the same sign.

In the clockwise rotation:

- Dyad trials: all of the elements of rPC1 have the same sign, indicating a similar activation (extending/flexing) of all of antagonistic muscle pairs (see Fig. 32).
- Single trials: the rPC1 vectors of each subject in single trials are different from the patterns they produced in the dyad trials (see Fig. 33).

2. PC2 vectors:

In the counterclockwise rotation:

- Dyad trials: the element corresponding to r_1 is different in sign compared to the others (see Fig. 30). Thus, for the movement in the radial direction, which is

Table 9: Percentage of variation accounted for by the first two PCs (A-A activity)

		Counterclockwise			Clockwise		
		PC1	PC2	Total	PC1	PC2	Total
Single trial	O	68.04	29.76	97.80	88.16	11.28	99.44
	S	66.71	23.44	90.15	79.36	14.51	93.87
Dyad trial	O	77.44	20.44	97.88	85.59	13.94	99.53
	S	55.11	36.67	91.78	61.90	33.55	95.45

related to rPC2, three antagonistic muscle pairs $\{r_2, r_3, r_4\}$ work in concert with each other and that is different from the pair r_1.

- Single trials: PC2 vectors of individuals are similar (see Fig. 31). The elements corresponding to $\{r_1, r_2\}$ are negative, the elements corresponding to $\{r_3, r_4\}$ are negative. These patterns are different from the patterns of each member in the dyad trials.

In the clockwise rotation:

- Dyad trials: the patterns of rPC2 vectors can be divided into two groups (see Fig. 32). One group is positive, and one group is negative. This pattern indicates that the two groups work in contrast with each other to produce the movement. In addition, the high value of the element corresponding to r_1 indicates a strong flexion of the shoulder joint.
- Single trials: the rPC2 vectors of each subject in single trials are different from the patterns of each other and are different from the patterns they produced in the dyad trials (see Fig. 33)

5.4.2 A-A activity

For both single task and dyad task, the first two PCs contributed over 90% to the percentage variation of the A-A activities of each subject (see Table 9). Therefore, it is reasonable to represent A-A activities by using the first two PCs.

5.4.2.1 PC scores

1. PC1 scores:

   - Dyad trials: PC1 scores of A-A activity of each dyad member were similar in shape. Figure 34 shows the PC1 scores (aPC1) of dyad OS in the counterclockwise rotation. They all have a similar shape but different in phase. In early practices, subject S's aPC1 are always phase lead. This pattern is active/inert pattern. The phase lead reduces through practices. This pattern is also valid for the clockwise rotation (see Fig. 36).
   - Single trials: For different movements, counterclockwise and clockwise movements, aPC1 score pattern of subject S changed while that of subject O kept the same (see Fig. 35 and 37). Moreover, aPC1 score pattern of subject O is similar to his aPC1 score pattern observed in the dyad trials.

2. PC2 scores:

   - Dyad trials: PC2 scores (aPC2) of each dyad member were similar. Figure 38 and 40 exhibit the aPC2 of dyad OS in dyad trials in the counterclockwise rotation and in the clockwise rotation, respectively. aPC2 of subject O is smoother than that of subject S in most of the trials.
   - Single trials: aPC2 score patterns of subject S in the counterclockwise rotation and in the clockwise rotation are different, and they are different from his aPC2 score pattern observed in the dyad trials. On the other hand, aPC2 score pattern of subject O kept the same.

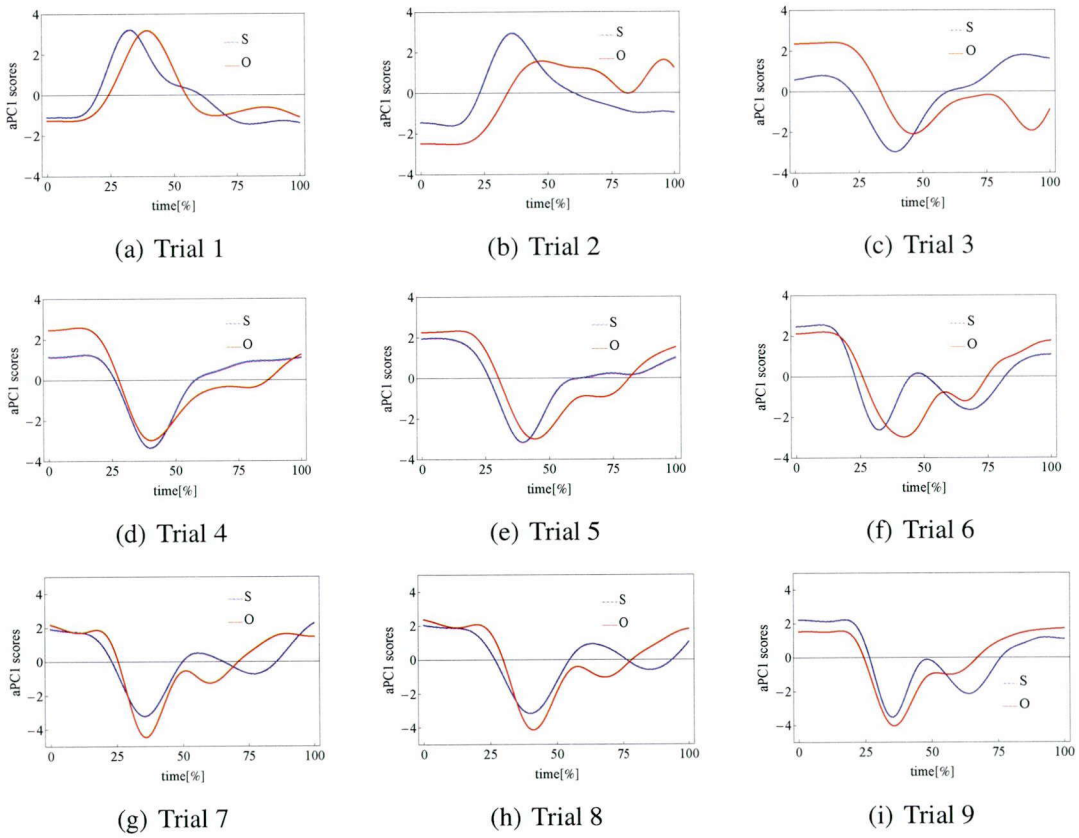

(a) Trial 1 (b) Trial 2 (c) Trial 3

(d) Trial 4 (e) Trial 5 (f) Trial 6

(g) Trial 7 (h) Trial 8 (i) Trial 9

Figure 34: PC1 scores of A-A activity of dyad trials in the counterclockwise rotation.

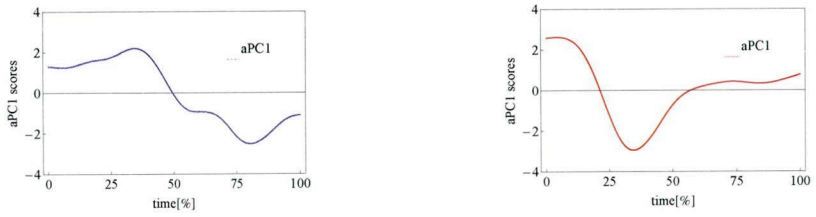

(a) Single S (b) Single O

Figure 35: PC1 scores of A-A activity of individuals in the counterclockwise rotation.

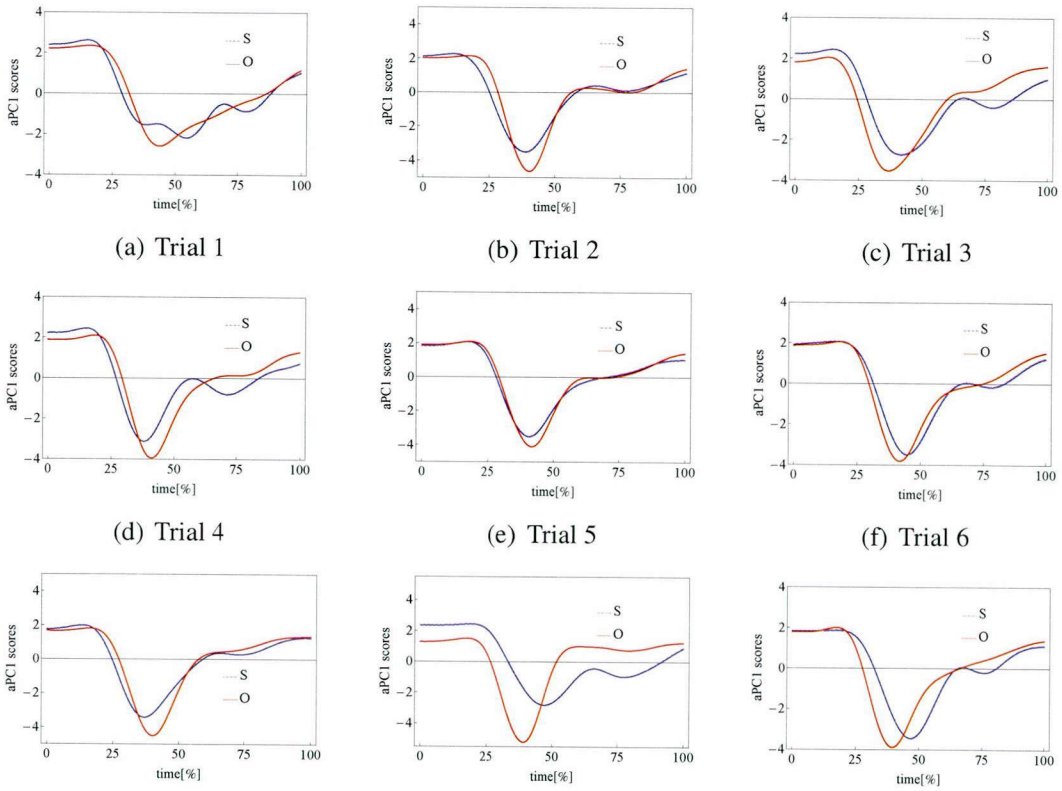

(a) Trial 1 (b) Trial 2 (c) Trial 3

(d) Trial 4 (e) Trial 5 (f) Trial 6

(g) Trial 7 (h) Trial 8 (i) Trial 9

Figure 36: PC1 scores of A-A activity of dyad trials in the clockwise rotation.

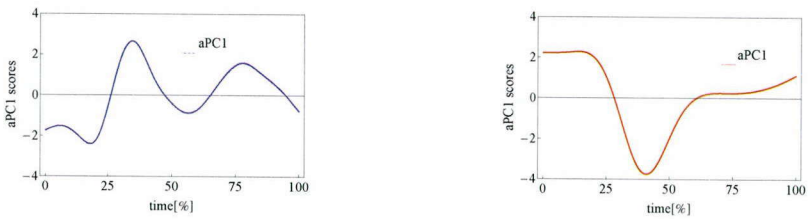

(a) Single S (b) Single O

Figure 37: PC1 scores of A-A activity of individuals in the clockwise rotation.

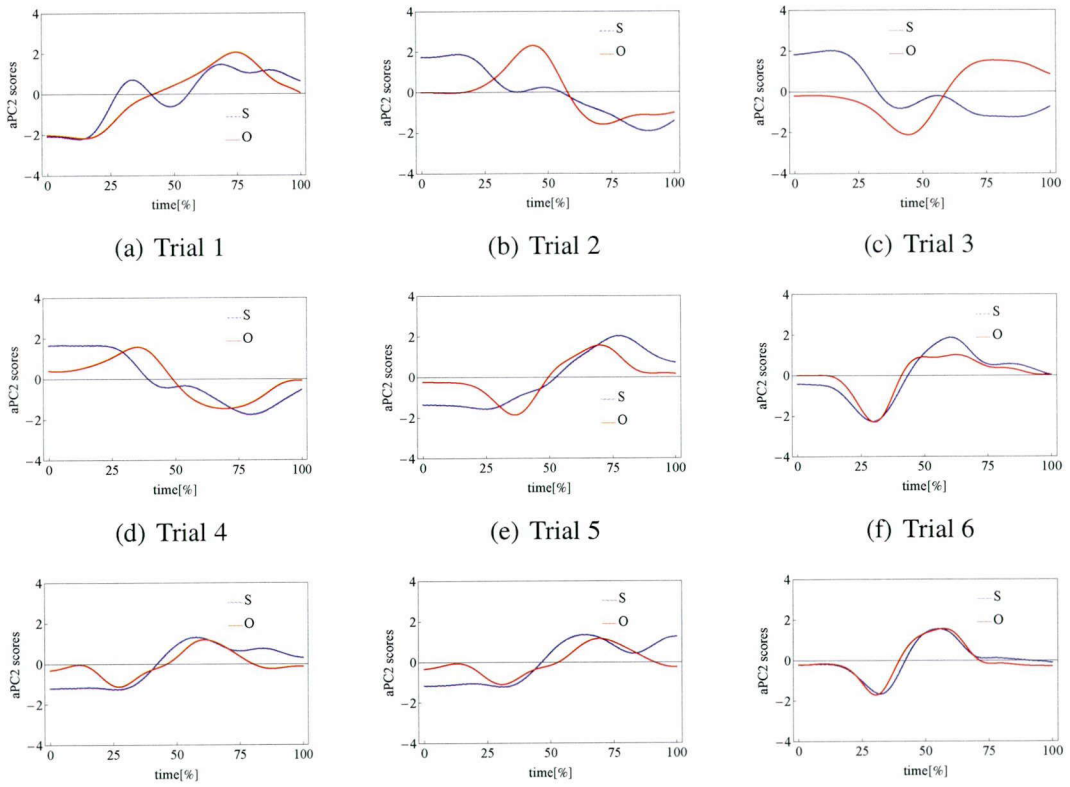

(a) Trial 1 (b) Trial 2 (c) Trial 3

(d) Trial 4 (e) Trial 5 (f) Trial 6

(g) Trial 7 (h) Trial 8 (i) Trial 8

Figure 38: PC2 scores of A-A activity of dyad trials in the counterclockwise rotation.

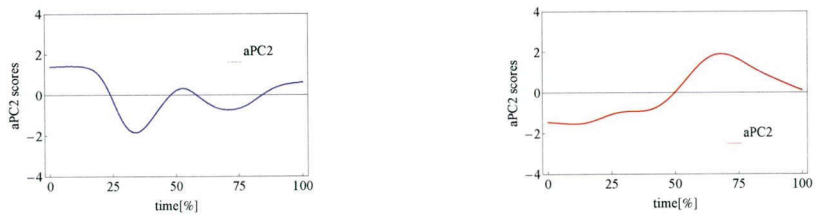

(a) Single S (b) Single O

Figure 39: PC2 scores of A-A activity of individuals in the counterclockwise rotation.

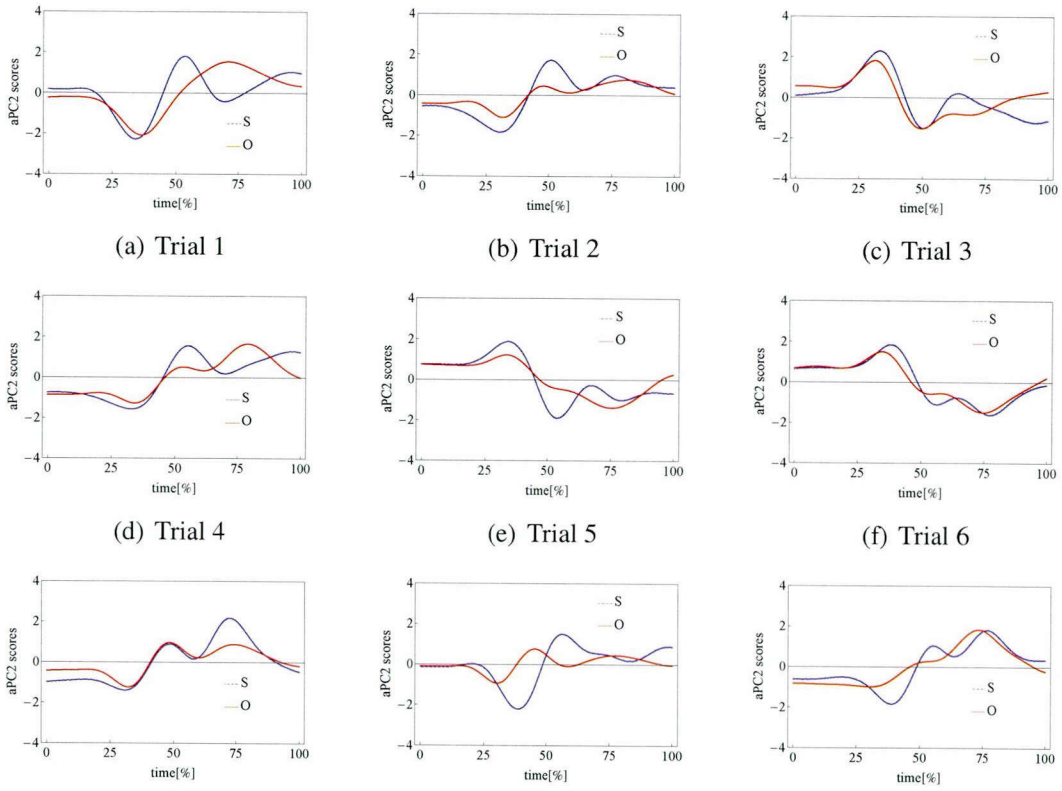

(a) Trial 1 (b) Trial 2 (c) Trial 3

(d) Trial 4 (e) Trial 5 (f) Trial 6

(g) Trial 7 (h) Trial 8 (i) Trial 9

Figure 40: PC2 scores of A-A activity of dyad trials in the clockwise rotation.

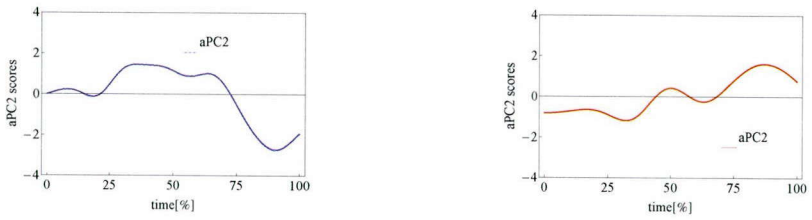

(a) Single S (b) Single O

Figure 41: PC2 scores of A-A activity of individuals in the clockwise rotation.

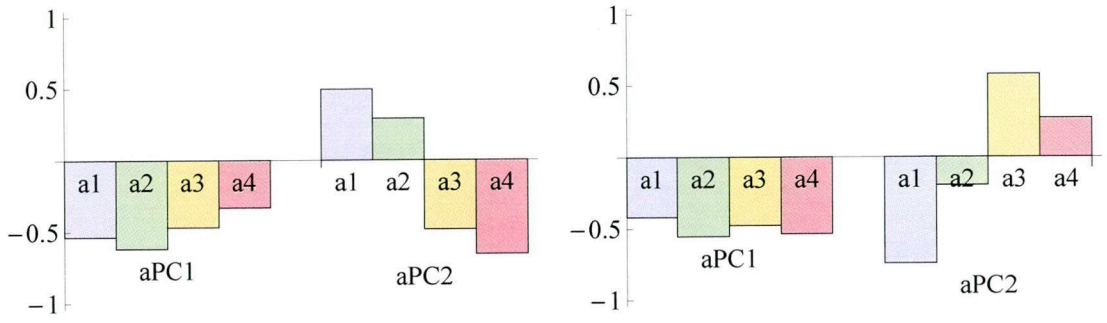

(a) Subject S (b) Subject O

Figure 42: PC vectors of A-A activity of dyad trials in the counterclockwise rotation.

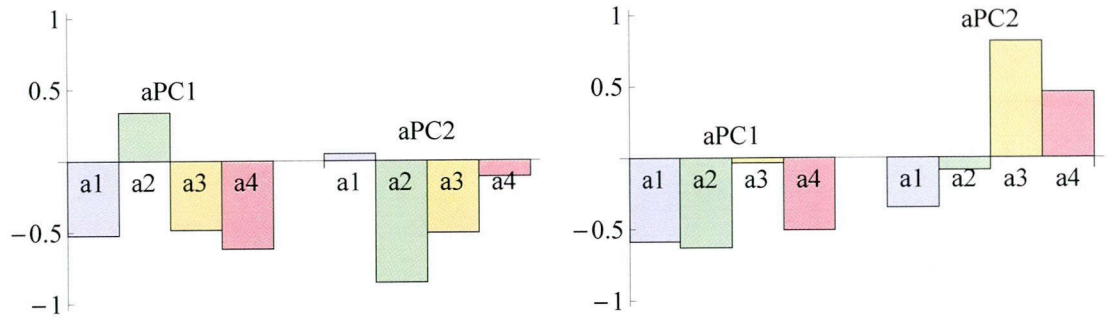

(a) Single S (b) Single O

Figure 43: PC vectors of A-A activity of individuals in the counterclockwise rotation.

5.4.2.2 PC vectors

The patterns of PC1 vectors of A-A activity (aPC1 vectors) of the two dyad members were similar in both counterclockwise rotation and clockwise rotation. Figure 42 and 44 present the aPC1 vectors of the dyad OS in the dyad trials in the counterclockwise rotation and in the clockwise rotation, respectively. aPC1 vector represents the major part of variation in the stiffness of the upper limb. All of its elements have the same sign, indicating that both of the subjects adjusted the stiffness concertedly. The values of elements of subject O's aPC1 are almost the same but those of subject S's aPC1 are not as stable as that, implying that subject O produced smoother movement as he controlled his stiffness smoother.

For aPC2 vector, in the counterclockwise rotation, the patterns of two dyad members were similar. Figure 42 shows the PC vectors of A-A activity in the dyad trials in the

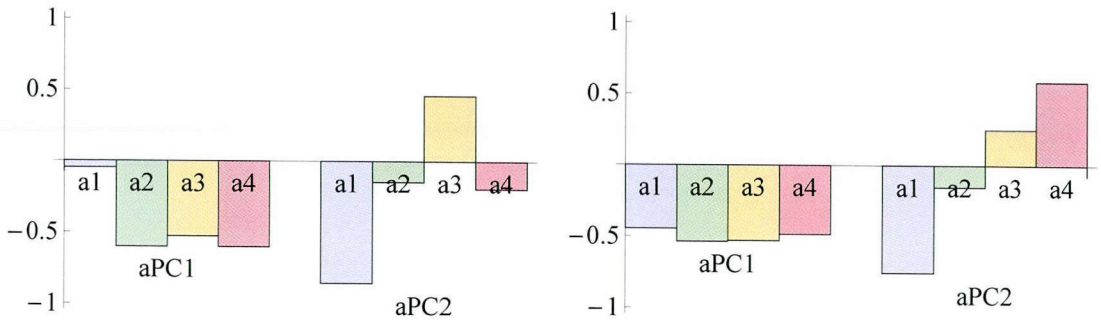

(a) Subject S (b) Subject O

Figure 44: PC vectors of A-A activity of dyad trials in the clockwise rotation.

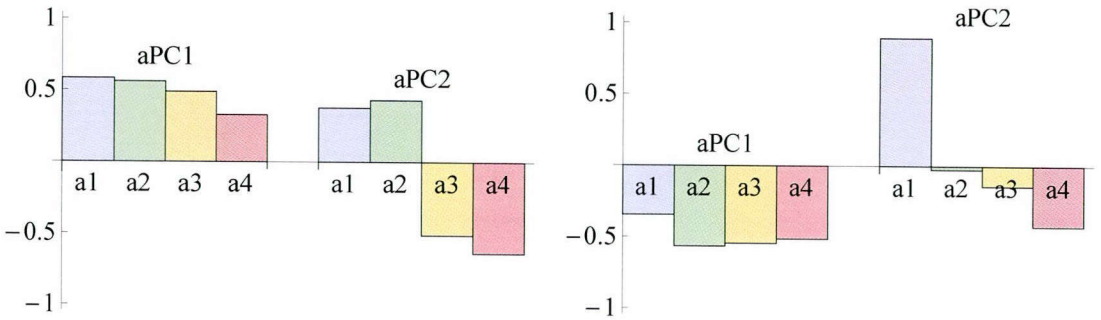

(a) Single S (b) Single O

Figure 45: PC vectors of A-A activity of individuals in the clockwise rotation.

counterclockwise rotation. As seen in this figure, the elements corresponding to $\{a_1, a_2\}$ are different sign with those corresponding to $\{a_3, a_4\}$, or the upper-arm's stiffness increases/decreases while the forearm's stiffness decreases/increases. In the clockwise rotation, however, aPC2 vector of two members are different. Subject S's aPC2 vector has three positive components and one negative component. Subject O's aPC2 vector stays the same as in the counterclockwise rotation, or he produced a similar stiffness in this task. In addition, the value of the element corresponding to a_1 is high, indicating a high stiffness of the shoulder joint.

The PC vectors of each subject in the single trials were different from each other's PC vectors and were different from his PC vectors in the dyad trials (see Fig. 43 and 45).

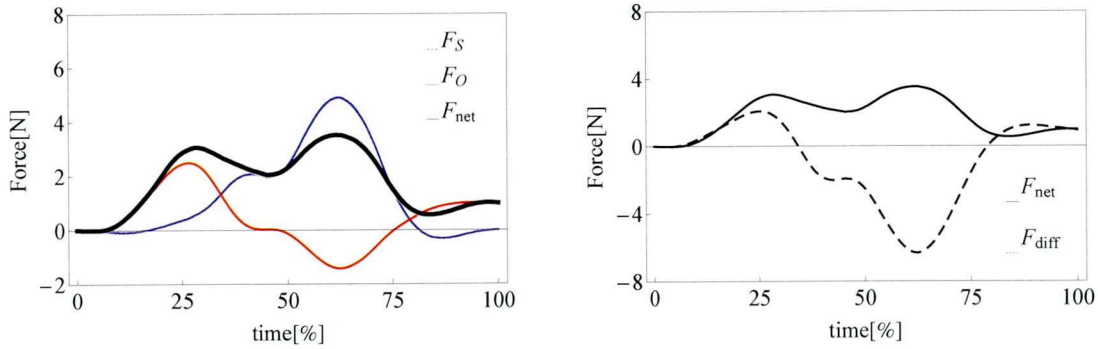

(a) (b)

Figure 46: Hand-force profiles in the counterclockwise rotation (dyad trial).

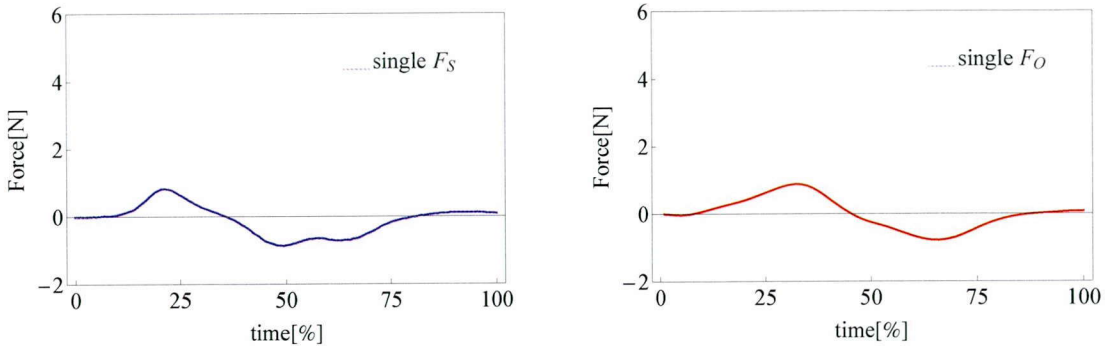

(a) S single trial (b) O single trial

Figure 47: Hand-force profiles in the counterclockwise rotation (single trial).

5.5 *Hand-force results*

Considering the tangential force, which is positive when placed towards the target, role divisions between two dyad members were observed. Call F_{net} the sum of each member's force, F_{diff} the difference force of the two members' forces. The net force F_{net} is the task-relevant force that accelerates the crank. The difference force has no physical effect on the crank motion. Two types of strategies were observed. Figure 46 shows the performance of dyad OS in the counterclockwise rotation. $F_{net} = F_O + F_S$ is the sum of subject O and subject S's forces in the dyad task. $F_{diff} = F_O - F_S$ is the difference force, measuring the

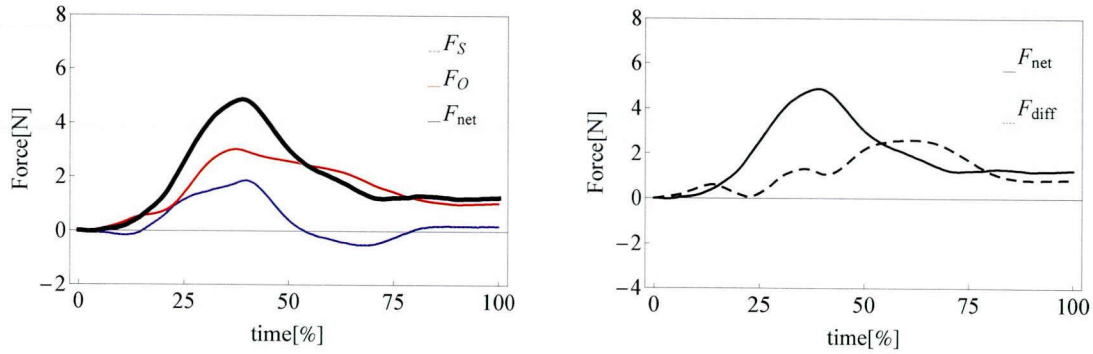

(a) Trial 3 (b) Trial 3

Figure 48: Hand-force profiles in the clockwise rotation (dyad trial).

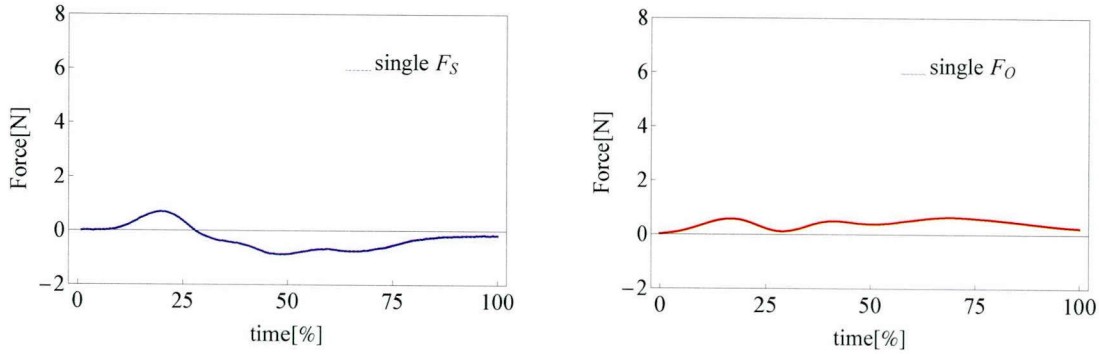

(a) S single trial (b) O single trial

Figure 49: Hand-force profiles in the clockwise rotation (single trial).

disagreement of the members. As seen in this figure, in early of the trial, subject O leads the crank movement while subject S performs a slow response. In the late half of the trial, subject S takes over the role of pushing the crank to move ($F_S > 0$) while subject O tries to decelerate the crank ($F_O < 0$). The difference force changes its sign. This performance is active/inert strategy. In the clockwise rotation, however, they demonstrated a different strategy. As seen in Fig. 48, both of the subjects solely push the crank towards the target. Subject O leads the movement. The difference force stays the same sign. This performance is similar to the specialized strategy.

The performance of the subjects in the dyad task was different from their performance in the single task. Call *singleF* the force of the individual in the single task. Figure 47(a) and 47(b) show that when working alone, both subject S and O present the acceleration strategy in the first half of the trial and the deceleration strategy in the late half of the trial. In the clockwise rotation, subject O simply pushes the crank towards the target (see Fig. 49(b)) while subject S performs a bang-bang type control (see Fig. 49(a)).

5.6 Discussion

Role divisions were observed by investigating the synergy variables. In the counterclockwise rotation, the rPC1 pattern, which is related to the movement in the angular direction, was a specialized pattern. That is, rPC1 of one subject was phase lead in the first half of the trial and rPC1 of the other subject was phase lead in the late half. However, in the clockwise rotation, rPC1 of one subject was always phase lead while rPC1 of the other subject followed. This pattern is an active/inert pattern. In contrast, rPC2, which results in the movement in the radial direction, was active/inert in the counterclockwise rotation and specialized in the clockwise rotation. On the other hand, role divisions can be approached by observing the hand-force profiles. In the counterclockwise rotation, one subject mainly pushed the crank in the first half of the trial while the other subject mainly produced force to move the crank in the late half of the trial (active/inert dyad). In the clockwise rotation, one subject led the movement while the other subject pulled along (specialized dyad). These roles observed from the hand-force profiles contrast with the roles observed from the patterns of rPC1 (the input of the angular-directional movement) but agree with the roles observed from the patterns of rPC2 (the input of the radial-directional movement).

In addition, the PC vectors of A-A ratio in the counterclockwise rotation and those in the clockwise rotation were different, or the activation level of each antagonist muscle pair was different at different movements. Moreover, the PC vectors of A-A activity can explain how the subjects distribute the stiffness over antagonistic muscle pairs. When the stiffness

was changed smoothly, the resultant performance observed was smooth.

Finally, the performance of dyad work was improved through trials. The synergy variables patterns also showed that in later trials, the phase lead decreased. It seemed that as practicing together, the dyad members tent to synchronize each other and adjusted their performance to work more compliantly with the partner. This fact may be the cause of the improvement in performance of the dyad work.

CHAPTER VI

CONCLUSION AND FUTURE WORK

This dissertation provides a method to extract, analyze, and implement muscle synergies to the upper-limb movement control. Here, we summary the conducted experiments and achievements.

First, we proposed A-A ratio and A-A activity concepts, setting the variables for analyzing the muscle synergies for movement generation of pneumatic artificial muscles systems as well as for human muscles. We provided a method to extract and to implement muscle synergies from A-A ratio of EMGs in a hand-force production task. The analysis based on the A-A ratio dataset was less tedious compared to the conventional analysis based on the original EMGs. The physical meanings of extracted muscle synergies were elucidated. That is, considering a polar coordinate system centered on the shoulder joint, one synergy seemed to generate hand-forces in the angular direction, while the other synergy seemed to create hand-forces in the radial direction. There have been some research that having a similar idea of using PC vectors and defining them as synergies. For example, Santello's work presented a method to obtain synergies from hand postures [28]. Our study, however, provides a way to identify synergies from muscle activities. The input for the analysis is more direct as muscle activities are the input of movements. In addition, they found that the first two principal components accounted for over 75%. Our method found the contribution of the first two principal components was over 90% (almost all cases), or our reduced data can represent the original data more significantly, thus, offering a better investigation on the data.

Second, we hypothesized a novel framework for motor control of the upper-limb movement. Using the hypothesized framework, we can explain the underlying procedure of

producing force. The proposed framework is a foothold to explain the mechanism to generate movements clearly. Furthermore, it enables us to make robots perform a wide range of tasks, such as a reaching task. In this dissertation, we demonstrated an implementation of the framework to control pneumatic-driven robots with synergy variables. There has been a few researches that transfer the characteristics of muscle activities to control musculoskeletal robots. Our work, however, proposes a synergy-based control method to control musculoskeletal robots. The simplicity and flexibility of the synergy control method make it a promising control method for high-redundant systems. It is applicable for other systems with more degrees-of-freedoms or to more complex tasks. In fact, we have tried it with pneumatic-driven leg robots that have 16 PAMs [44] and with movement in 3-dimensional space [33].

Finally, we investigated the performance of two people in a crank-cooperation task. Role divisions were observed in the dyad performance, suggesting the mechanisms that improve the dyad work. The observed role sharing would be helpful to improve the performance of musculoskeletal robots that involve in interaction tasks with human.

For future plan, it is necessary to deeply investigate the stiffness that is reflected by the A-A activity to optimize the relationship between the input (synergy variables) and the output (hand movements). The experiment to observe the coordinated performance between two human subjects should be conducted with more subjects so as to provide fruitful information, making the observation more reliable. In addition, the performance of dyad task should be validated with robot performance.

APPENDIX A

EXPERIMENT DEVICES AND THEIRS SPECIFICATIONS

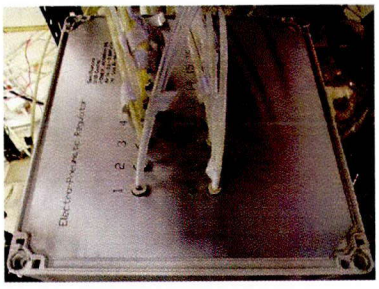

Figure 50: Electro-Pneumatic regulator

Figure 51: Air compressor

Table 10: Specifications of electro-pneumatic regulator

Name	APC-C300-16
Output ports	16
Max pressure	0.7 [MPa]
Control pressure range	0~0.5 [MPa]
Interface	Single-ended 0~10 [V]

Table 11: Specifications of air compressor

Name	JUNAIR 12-25
Output	0.80 [kW]
Maximum pressure	0.80 [MPa]
Air delivery	120 [liters/min]
Tank size	25 [liters]

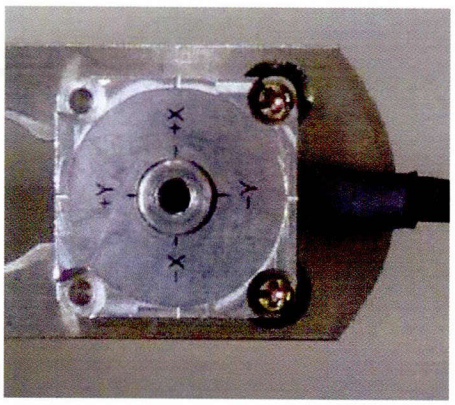

Figure 52: Force sensor

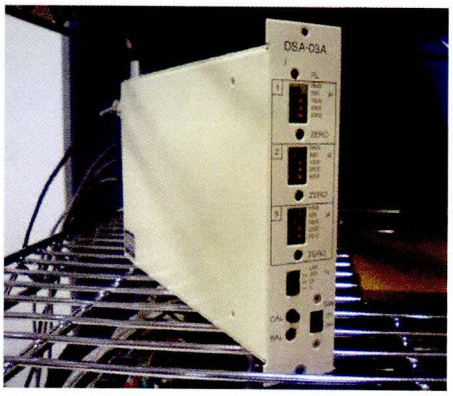

Figure 53: Force sensor's conditioner

Table 12: Specifications of force sensor

Name	USL06-H5-200N
Load range F_x, F, y	±100 [N]
Load range F_z	200 [N]
Nonlinearity	within 1.0% RO
Hysteresis	within RO
Operating temperature	10~60 [°C]
Overload	120%
Recommended voltage	1~3 [V]

Table 13: Specifications of calibration tool

Name	DSA-03A
Measurement channels	3
Sensor application	120~350 [Ω]
Applied voltage	DC 2.5 [V]
Zero adjustment range	+500 [$\mu\varepsilon$]
Low-pass filter	5, 20, 200 [Hz]
Output voltage	±5 [V]
Nonlinearity	±0.1% [FS]
Operating temperature	0~50 [°C]

Figure 54: WEB-5000 receiver

Figure 55: WEB-5000 transmitter

Table 14: Specifications of EMG measuring sets

Name	WEB-5000
Number of measurement channels	8
Wide cut-off frequency	100 [Hz]
Low-pass time constant	0.03, 0.01 [sec]
Sensitivity	0.2, 0.5, 1 [mV]
Max input	±5 [mV]
Noises	42 [μV]

Table 15: Specifications of A/D converter

Name	PCI-3346A
Conversion time	10 [μs]
Interface	Flat cable 50 Pin
Output channels	16
Output method	Unipolar
Input voltage range	0~10 [V]

Table 16: Specifications of A/D converter

Name	PCI-3522A
Conversion time	10 [μs] (fixed channel)
Conversion time	60 [μs] (switching channel)
Interface	Flat cable 50 Pin
Output channels	8
Output method	Single-ended
Input voltage range	0~10 [V]

REFERENCES

[1] A. D'Avella, A. Portone, L. Fernandez, and F. Lacquaniti, "Control of Fast-Reaching Movements by Muscle Synergy Combinations," *The Journal of Neuroscience*, vol. 26, pp. 7791–7810, July 2006.

[2] A. D'Avella and E. Bizzi, "Shared and specific muscle synergies in natural motor behaviours," *Proceeding of National Academy of Science of the United States of America*, vol. 102, no. 8, pp. 3076–3081, 2005.

[3] A. D'Avella, P. Saltiel, and E. Bizzi, "Combinations of muscle synergies in the construction of a natural motor behavior," *Nature Neuroscience*, vol. 6, pp. 300–308, 2003.

[4] A.G. Feldman, "Functional tuning of the nervous system with control of movement or maintenance of a steady posture. II. Controllable parameters of the muscle," *Biophysics*, vol. 11, pp. 565–578, 1966.

[5] A.G. Feldman, "Superposition of motor programs. I. Rhythmic forearm movements in man," *Neuroscience*, vol. 5, pp. 81–90, 1980.

[6] C. Chou and B. Hannaford, "Measurement and modeling of Mckibenn pneumatic artificial muscle," *IEEE Transactions on Robotics and Automation*, vol. 12, no. 1, pp. 90–102, 1996.

[7] D. Maeda, K. Tominaga, T. Oku, H. Pham, S. Saeki, M. Uemura, H. Hirai, and F. Miyazaki, "Muscle synergy analysis of human adaptation to a variable-stiffness exoskeleton: human walk with a knee exoskeleton with pneumatic artificial muscles," IEEE/RAS International Conference on Humanoid Robots, 2012.

[8] D. Shin, J. Kim, and Y. Koike, "A myokinetic arm model for estimating joint torque and stiffness from EMG signals during maintained posture," *J Neurophysiol.*, vol. 101, no. 1, pp. 387–401, 2012.

[9] D.L. Turner, P. Sacco, and T. Hunter, "Complex motor cortex control of muscle synergies underpin simple reaching tasks in robot-induced force fields," 2008.

[10] D.R. Humphrey, "Separate cell systems in the motor cortex of the monkey for the control of joint movement and of joint stiffness," *Electroencephalogr and clinical neurophysiol. Supplement*, vol. 36, pp. 393–408, 1982.

[11] E. Bizzi, A. d'Avella, P. Saltiel, and M. Tresch, "Modular organization of spinal motor systems," *Neuroscientist*, vol. 8, pp. 437–422, 2002.

[12] E. Bizzi, V.C.K. Cheung, A. d'Avella, P. Saltiel, and M. Tresch, "Combining modules for movement," *Brain research reviews*, vol. 57, pp. 125–133, 2008.

[13] F. Lacquaniti and C. Maioli, *Distributed control of limb position and force*. 1992.

[14] G.L. Gottlieb, "Muscle activation patterns during two types of voluntary single-joint movement," *Journal of Neurophysiology*, vol. 80, pp. 1860–1867, 1998.

[15] H. Hirai, T. Iimura, K. Mitsumori, and F. Miyazaki, "Modular control of limb kinematics during human walking," pp. 716–721, IEEE/RAS-EMBS International Conference on Biomedical Robotics and Biomechatronics (BioRob 2010), 2010.

[16] H. Hislop and J. Montgomery, *Daniels Worthingham's Muscle Testing: Techniques of Manual Examination*. Saunders, 8 ed.

[17] H. Pham, M. Kimura, H. Hirai, and F. Miyazaki, "Extraction and implementation of muscle synergies in hand-force control," pp. 3658–3663, IEEE International Conference on Robots and Automation (ICRA2011), 2011.

[18] I. Jolliffe, *Principal components analysis*. New York: Springer Verlag, 1986.

[19] J. M. Macpherson, *How flexible are muscle synergies?* John Wiley and Sons Ltd, 1991.

[20] K. Inoue, T. Iimura, T. Oku, H. Pham, H. Hirai, and F. Miyazaki, "An experimental study of muscle coordination and function during human locomotion," vol. 1, BIO Web of Conferences/ The International Conference SKILLS, 2011.

[21] K. Reed, James Patton, Michael Peshkin, "Replicating Human-Human Physical Interaction," pp. 3615–3620, Proc. of IEEE International Conference on Robotics and Automation (ICRA), 2007.

[22] K. Reed, M. Hartmann, J. Patton, P. Vishton, M. Grabowecky, and M. Peshkin, "Haptic cooperation between people, and between people and machines," pp. 2109–2114, Proc. of IEEE International Conference on Intelligent Robots and Systems (IROS), 2006.

[23] K. Reed, M. Peshkin, J. Colgate, and J. Pattonl, "Initial Studies in Human-Robot-Human Interaction : Fitts' Law for Two People," vol. 3, pp. 2333–2338, Proc. of IEEE International Conference on Robotics and Automation (ICRA), 2004.

[24] K.B. Reed, "Physical collaboration of human-human and human-robot teams," *IEEE Transactions on Haptics*, vol. 1, pp. 108–120, 2008.

[25] L. H. Ting and J. L. McKay, "Neuromechanics of muscle synergies for posture and movement," *Current Opinion in Neurobiology*, vol. 17, pp. 622–628, 2007.

[26] L.H. Ting, *Dimensional reduction in sensorimotor systems: a framework for understanding muscle coordination of posture*, vol. 165, ch. 19, pp. 299–321. Progress in Brain Research, 2007.

[27] M. Azegami, R. Yanagihashi, K. Miyoshi, K. Akahane, M. Ogira, and T. Sadoyama, "Effects of multi-joint angle changes on EMG activity and force of lower extremity muscles during maximum isometric leg press exercises," *J. Phys. Ther. Sci.*, vol. 19, pp. 65–72, 2007.

[28] M. Santello, M. Flanders, and J. F. Soechting, "Patterns of hand motion during grasping and the influence of sensory guidance," *The Journal of Neuroscience*, vol. 22, pp. 1426–1435, 2002.

[29] M.C. Tresch and A. Jarc, "The case for and against muscle synergies," *Current Opinion in Neurobiology*, pp. 601–607, 2009.

[30] M.L. Latash, "Evolution of motor control: from reflexes and motor programs to the equilibrium-point hypothesis," *Journal of Human Kinetics*, vol. 19, no. 19, pp. 3–24, 2008.

[31] M.L. Latash, *Neurophysiological basis of movement.* Human Kinetics, 2008.

[32] N. Bernstein, *The coordination and regulation of movements.* Oxford: Pergamon Press, 1967.

[33] N. Hasegawa, M. Uemura, H. Hirai, and F. Miyazaki, "Muscle synergy analysis of human arm movement in a three-dimensional reaching task," Proc. of SICE Symp. on System Integration, 2012 (in Japanese).

[34] N. Hogan, "The mechanics of multi-joint posture and movement control," *Biological Cybernetics*, vol. 52, no. 5, pp. 315–331, 1985.

[35] O. Levin, M. Ouamer, M. Steyvers, and S.P. Swinnen, "Directional tuning effects during cyclical two-joint arm movements in the horizontal plane," *Experimental Brain Research*, vol. 141, pp. 471–484, 2001.

[36] P.K. Artemiadis and K.J. Kyriakopoulos, "EMG-Based Control of a Robot Arm Using Low-Dimensional Embeddings," *IEEE Transactions on Robotics*, pp. 393–398, 2010.

[37] R. Ueha, H. Pham, H. Hirai, and F. Miyazaki, "A simple control design for human-robot coordination based on the knowledge of dynamical role division," IEEE/RSJ International Conference on Intelligent Robotics and Systems (IROS), 2009.

[38] R.A. Schmidt and C.A. Wrisberg, *Motor Learning and Performance.* Human Kinetics, 2004.

[39] S. Arimoto and F. Miyazaki, "Bettering operation of robots by learning," *Journal of Robotic Systems*, vol. 1, no. 2, pp. 123–140, 1984.

[40] S. Fujimoto, T. Ono, K. Ohsaka, and Z. Zhao, "Modeling of artificial muscle actuator and control design for antagonistic drive system," *Transactions of the Japan Society of Mechanical Engineers*, vol. 73, no. 730, pp. 1777–1785, 2007.

[41] S. Giszter, V. Patil, and C. Hart, "Primitives, premotor drives, and pattern generation: a combined computational and neuroethological perspective," *Progress in Brain Research*, vol. 165, pp. 323–346, 2007.

[42] T. Drew, J. Kalaska, and N. Krouchev, "Muscle synergies during locomotion in the cat: a model for motor cortex control," *J Physiol*, vol. 586, no. 5, pp. 1239–1245, 2008.

[43] T. Iimura, K. Inoue, H. Pham, H. Hirai and F. Miyazaki, "Decomposition of limb movement based on muscular coordination during human running," *Journal of Advanced Computational Intelligence and Intelligent Informatics*, vol. 15, pp. 980–987, 2011.

[44] T. Oku, K. Inoue, H. Pham, K. Tominaga, D. Maeda, M. Uemura, H. Hirai, and F. Miyazaki, "Analysis of muscle coordination in human pedaling and implementation with a musculoskeletal robot," IEEE/RAS International Conference on Humanoid Robots, 2012.

[45] T.E. Milner, C. Cloutier, A.B. Leger, and D.W. Franklin, "Inability to activate muscles maximally during cocontraction and the effect on joint stiffness," *Experimental Brain Research*, vol. 107, pp. 293–305, 1995.

[46] W. A. Lee, "Neuromotor synergies as a basis for coordinated intentional action," *Journal of Motor Behavior*, vol. 16, pp. 135–170, 1984.

[47] Y. Ariga, H. Pham, M. Uemura, H. Hirai, and F. Miyazaki, "Novel equilibrium-point control of agonist-antagonist system with pneumatic artificial muscles," IEEE International Conference on Robotics and Automation (ICRA), 2012.

[48] Y. Honda, F. Miyazaki, A. Nishikawa, "Control of pneumatic five-fingered robot hand using antagonistic muscle ratio and antagonistic muscle activity," pp. 337–342, International Conference on Biomedical Robotics and Biomechatronics (BioRob), 2010.

[49] Y.P. Ivanenko, R.E. Popplele, and F. Lacquaniti, "Five basic muscle activation patterns account for muscle activity during human locomotion," *Journal of Physiology*, vol. 556, no. 1, pp. 267–282, 2004.

LIST OF PUBLICATIONS

Journals

1. H. Pham, M. Hazada, D. Maeda, H. Hirai, and F. Miyazaki, "Muscle synergy extraction in a hand-force control and its implementation in robot control," *Journal of Japan Society for Fuzzy Theory and Intelligent Informatics*, vol. 24, No. 1, pp. 536–544, 2011.

2. T. Iimura, K. Inoue, H. Pham, H. Hirai, and F. Miyazaki, "Decomposition of limb movement based on muscular coordination during human running," *Journal of Advanced Computational Intelligence and Intelligent Informatics*, 15, pp. 980–987, 2011.

3. Y. Ariga, D. Maeda, H. Pham, K. Nakayama, M. Uemura, H. Hirai, and F. Miyazaki, "The linear control of antagonistic-driven system using A-A ratio and A-A activity and its application to the EMG interface," *Journal of the Robotics Society of Japan*, vol. 31, No. 4.

4. H. Pham, Y. Ariga, M. Kimura, M. Uemura, H. Hirai, and F. Miyazaki, "Extraction and implementation of muscle synergies in neuro-mechanical control of upper limb movemen," *IEEE Transactions on Robotics*, 2012 (submitted).

Conferences

1. R. Ueha, H. Pham, H. Hirai, and F. Miyazaki, "Dynamical role division between two subjects in a crank-rotation task," IEEE 11th International Conference on Rehabilitation Robotics (ICORR), 2009.

2. R. Ueha, H. Pham, H. Hirai, and F. Miyazaki, "A simple control design for human-robot coordination based on the knowledge of dynamical role division," IEEE/RSJ International Conference on Intelligent Robotics and Systems (IROS), 2009.

3. H. Pham, Y. Honda, Y. Ariga, H. Hirai, and F. Miyazaki, "A high correlation estimation of hand-force based on muscle activities," The Conference of Robotics Society of Japan, 2010.

4. H. Pham, R. Ueha, H. Hirai, and F. Miyazaki, "Extraction and implementation of muscle synergies in hand-force control," IEEE International Conference on Robotics and Automation (ICRA), pp. 3658–3663, 2011.

5. H. Pham, R. Ueha, H. Hirai, and F. Miyazaki, "A study on dynamical role division in a crank-rotation task from the viewpoint of kinetics and muscle activity analysis," pp. 2188–2193, International Conference on Intelligent Robotics and Systems (IROS), 2010.

6. K. Inoue, T. Iimura, T. Oku, H. Pham, H. Hirai, and F. Miyazaki, "An experimental study of muscle coordination and function during human locomotion," vol. 1, BIO Web of Conferences/ The International Conference SKILLS, 2011.

7. T. Iimura, K. Inoue, H. Pham, M. Uemura, H. Hirai, and F. Miyazaki, "A preliminary experiment for transferring human motion to a musculoskeletal robot-Decomposition of human running based on muscular coordination," IEEE/RSJ International Conference on Intelligent Robotics and Systems (IROS), pp. 4496–4501, 2011.

8. Y. Ariga, M. Uemura, H. Hirai, and F. Miyazaki, "Novel equilibrium-point control of agonist-antagonist system with pneumatic artificial muscles," IEEE International Conference on Robotics and Automation (ICRA), 2012.

9. T. Oku, K. Inoue, H. Pham, K. Tominaga, D. Maeda, M. Uemura, H. Hirai, and F. Miyazaki, "Analysis of muscle coordination in human pedaling and implementation with a musculoskeletal robot," IEEE/RAS International Conference on Humanoid Robots, 2012.

10. D. Maeda, K. Tominaga, T. Oku, H. Pham, S. Saeki, M. Uemura, H. Hirai, and F. Miyazaki, "Muscle synergy analysis of human adaptation to a variable-stiffness exoskeleton: human walk with a knee exoskeleton with pneumatic artificial muscles," IEEE/RAS International Conference on Humanoid Robots, 2012.

11. Y. Ariga, D. Maeda, H. Pham, M. Uemura, H. Hirai, and F. Miyazaki, "Novel equilibrium-point control of agonist-antagonist system with pneumatic artificial muscles: II. Application to EMG-based human-machine interface for an elbow-joint system," IEEE/RSJ International Conference on Intelligent Robotics and Systems (IROS), 2012.